Agilent

Trusted Answers

Live Cell Proliferation and Viability

Application Compendium

Table of Contents

Introduction

Counting the number of viable cells in a sample is a key step in many biological assays from normalization to measuring the effects of drugs on cell proliferation.[1,2] Routine maintenance of cell culture also involves monitoring cell growth and counts for consistent cell seeding densities for downstream experiments. For live cell assays where proliferation is a key indicator of effectiveness, a non-destructive or label-free method of counting cells is desirable. Alternatively, destructive measures can be used, the most straightforward of which is to harvest cells and use a counting chamber for quantification. Other examples of destructive or end point methods include measuring proxies of cell number such as total protein (e.g. BCA) and cellular metabolism (e.g. MTT, CellTiter-Glo).[3,4] However, this strategy requires multiple replicates per time point and is not conducive to high-throughput studies.

High-throughput counting of viable cells is a problem that has found many solutions over the years. With high-throughput microscopy instruments becoming more common, the direct counting of cells is a more accurate method for determining cell number and density (multinucleated cells excepted). The use of fluorescent stains or fluorescent proteins (nuclear locating sequence or histone labels) to label live and dead cells is common for short-term or end point assays.[5] In addition, stains marking apoptosis or necrosis provide even more detail about the non-viability of cells.

However, common DNA live cell stains (e.g. Hoechst 33342 and DRAQ5) can interfere with cell division disrupting the proliferation kinetics. Additionally, with Hoechst 33342, UV excitation of the dye is directly toxic to cells.[6] Furthermore, a direct brightfield or phase contrast measurement of confluence can mask total cell number, as cells adapt their volume with the amount of available culture space. High-contrast brightfield is a technique that increases contrast by brightfield illumination with a pinhole to give additional contrast to cell bodies, particularly in the area around the nucleus.[7] Label-free cell counting using high-contrast brightfield quantifies a direct count of cells with this increased contrast. Most adherent cells and many non-adherent cells show a high-contrast brightfield signal for a label-free cell counting method (Figure 1). By counting cell nuclei, a more accurate picture of cell proliferation is presented without using fluorescent dyes.

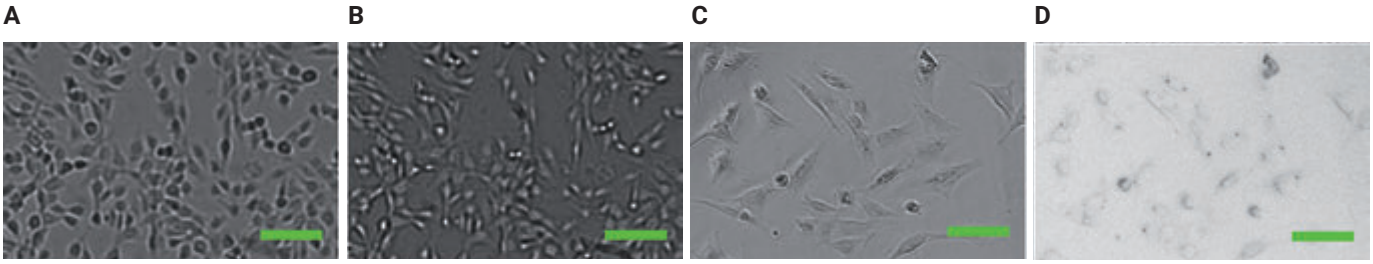

Figure 1. ANIH3T3 cells imaged at 4x on an Agilent BioTek Lionheart FX automated microscope using high-contrast brightfield (A,B), phase contrast (C), and standard brightfield (D). The slightly defocused image in (B) shows the increased contrast used for label- free cell counting. Scale bar, 100 µm.

In this application compendium, several experiments concerning cell proliferation and viability are presented using the Agilent BioTek Lionheart FX automated microscope and the Agilent BioTek Cytation cell imaging multimode reader. Kinetic monitoring of cell proliferation as a response to drug treatment is an example of label-free cell counting in the context of a proliferation-inhibiting drug. Additional experiments combine the label-free counting with markers of cell death, including apoptosis and necrosis, to give a broader picture of the effects of drug treatment on cell viability. For accurate seeding of cell experiments, an experiment is presented on automated cell counting and viability using the Agilent BioTek Cell Count and Viability Starter Kit. Finally, non-animal cell imaging is demonstrated by counting and measuring yeast proliferation with brightfield microscopy.

Instrumentation

Agilent BioTek Lionheart FX automated microscope

The Agilent BioTek Lionheart FX automated microscope is a compact, inclusive microscopy system for a broad range of imaging workflows. It has up to 60x air; 60x and 100x oil immersion magnification, with fluorescence, brightfield, color brightfield, and phase contrast channels for maximum application reach. Environment controls including incubation to 40 °C, CO_2/O_2 control and a humidity chamber optimize conditions for kinetic live cell imaging applications.

Agilent BioTek Cytation 5 cell imaging multimode reader

The Agilent BioTek Cytation 5 cell imaging multimode reader combines automated digital microscopy and conventional microplate detection in a configurable, upgradable platform. The microscopy module offers up to 60x magnification in fluorescence, brightfield, high-contrast brightfield, color brightfield and phase contrast imaging; temperature control to 65 °C and CO_2/O_2 control facilitates live cell imaging workflows.

Agilent BioTek BioSpa live cell analysis system

The Agilent BioTek BioSpa live cell analysis system is configured with the Agilent BioTek BioSpa 8 automated incubator and the Agilent BioTek Cytation cell imaging multimode reader to automate kinetic live cell analysis workflow in up to eight microplates or other labware. Temperature and CO_2/O_2 control, plus humidity monitoring support live cell imaging workflows. Liquid handling can be integrated for further process automation.

Cellular Proliferation and Viability Applications

Kinetic proliferation assay using label-free cell counting

Assay principle

Characterizing cell proliferation is a crucial aspect of biological research and therapeutic drug development. Most current cell proliferation assays rely on indirect biochemical metrics that are limited by artifacts or imaging-based end point measures. Here, we describe a continuous live cell assay for determining cell proliferation profiles using the BioSpa 8 and Cytation 5 with the High Contrast Brightfield Kit. This fully automated method enables accurate quantitative and phenotypic long-term analysis of cell growth using label-free direct cell counting.[7]

The High Contrast Brightfield Kit causes refraction of light by each cell to produce a bright spot, enabling accurate cell counting without the need for nuclear staining (Figure 2).

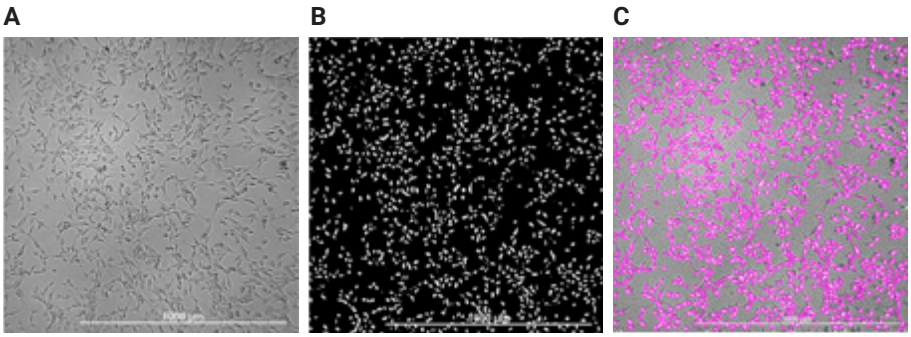

Figure 2. High-contrast brightfield direct cell counting. (A) In focus image of NIH3T3 cells. (B) Defocused image produces a single bright spot corresponding to each cell. (C) Agilent BioTek Gen5 microplate reader and imager software object masking tool can readily identify each bright spot to generate cell counts.

High-contrast brightfield cell counts are comparable to counts achieved using nuclear dyes, such as Hoechst and DAPI (Figure 3), while enabling long-term proliferation studies.[8]

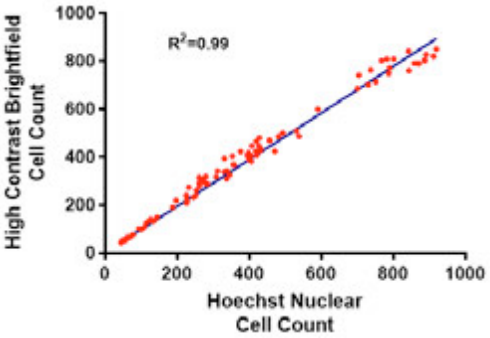

Figure 3. Comparison of high-contrast brightfield label-free cell counting to cell counts using Hoechst labeled nuclei. Cell counts of Hoechst stained NIH3T3 cells from the two techniques were highly comparable across a wide range of seeding densities. Points were fitted to a nonlinear regression equation with an R2 value of 0.99 and a slope of 0.97.

NIH3T3, HCT116, and HeLa cell growth was monitored for five days. All three cell types exhibited robust logarithmic growth up to full confluence. To demonstrate the ability of this system to screen pharmacological agents, cell proliferation profiles for cells cultured with eight concentrations of two anti-cancer drugs were generated. Concentration-response curves and IC_{50} values were used to quantify anti-proliferation effects for each cell type.

Materials and methods

Cell culture

NIH3T3 and HeLa cells were grown in Advanced Dulbecco's Modified Eagle's Medium (DMEM) (Gibco, Grand Island, NY) with 10 % FBS (Gibco), and 1x PenStrep-Glutamine (Cellgro, Manassas, VA). HCT116 cells were grown in McCoys 5A medium (Gibco) with 10 % FBS, and 1x PenStrep-Glutamine. Cells were seeded into black sided clear bottom 96-well microplates (Corning, Corning, NY) at 2000 cells per well. Environmental conditions, including temperature (37 °C), gas (5 % CO_2) and humidity (90 %) were maintained during the five day incubation by a BioSpa 8.

Cell imaging

Two high-contrast brightfield images were captured at each time point: an in focus image used for reference, and a defocused image for cell counting.[9] Briefly, cells were brought into focus using the High Contrast Brightfield Kit and the "in focus" focal height recorded. The Line Profile tool was then used to draw a line that crossed cells and background sections of the imaging field without cells present. The focal height was then decreased while observing the line profile to determine the focal height at which maximum contrast between cell and background brightness was achieved.

Image analysis

Image preprocessing was used to obtain the best possible enhancement of contrast, reducing each cell to a single bright spot. Object masking thresholds were then set to identify each cell for counting (Table 1).

Image Preprocessing	
Image Set	Brightfield_2
Background	Dark
Rolling Ball Diameter	20 µm
Image Set	3 cycles of 3x3 average filter
Cellular Analysis Parameters	
Channel	Tsf[Brightfield_2]
Threshold	5000
Background	Dark
Split Touching Objects	Checked
Fill Holes in Mask	Checked
Minimum Object Size	5 µm
Maximum Object Size	100 µm
Include Primary Edge Objects	Unchecked
Analyze Entire Image	Checked
Advanced Analysis Parameters	
Rolling Ball Diameter	50 µm
Image Smoothing Strength	1 cycle of 3x3 average filter
Evaluate Background On	5 %
Primary Mask	Use threshold mask

Table 1. Agilent BioTek Gen5 microplate reader and imager software setting. Image preprocessing improves contrast reduces background. Cellular analysis parameters and advanced analysis parameters are set to optimize identification of each cell for accurate cell counts.

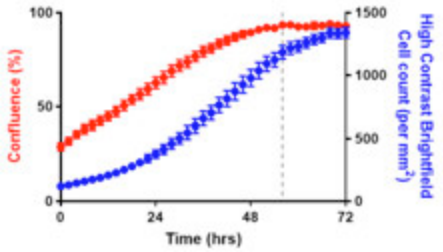

Figure 4. High-contrast brightfield cell counts over time relative to confluence. A comparison of NIH3T3 direct cell counts and percent confluence over time demonstrate the different characteristics of the two-cell growth metrics. Label-free cell counts indicate robust logarithmic cell growth up to full confluence (dashed line).

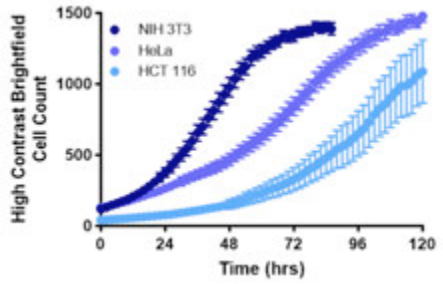

Figure 5. Label-free direct cell count profiles for NIH3T3, HeLa and HCT116. Cells were imaged every two hours and culture growth was monitored for five days or until cell counts plateaued.

Results and discussion

Quantitative evaluation of cell proliferation using label-free direct cell counting

Label-free methods of measuring cell growth kinetics are preferable over the use of stains that can influence proliferation rates. Although confluence level can be used for some applications, cell counting is the most direct quantitative measure of cell proliferation over a broad range of cell population densities (Figure 4).

Comparison of cell proliferation profiles across three cell types

NIH3T3, HeLa, and HCT116 cells were seeded at low densities and incubated in a BioSpa 8 for five days. High-contrast brightfield cell counts were used to define proliferation profiles for each cell type (Figure 5). All cells exhibited robust logarithmic growth under these conditions up to full confluence.

Measuring effect of anti-proliferation compounds on cell growth rates

Kinetic cell proliferation studies enable quantitative evaluation of cancer therapeutics. Doxorubicin is an anthracycline antitumor antibiotic that interrupts cell division by intercalating DNA and inhibiting macromolecular biosynthesis.[10, 11] It is commonly used in the treatment of a broad range of cancers.[10] Cercosporamide is a MAPK-interacting kinase (Mnk) that is a potent and selective inhibitor of the translation initiation factor 4E (eIF4E).[12] Recent studies have reported cercosporamide inhibits malignant tumor outgrowth, including HCT116 colon carcinoma xenograft tumors.[12, 13] To explore the effect of doxorubicin and cercosporamide on NIH3T3, HeLa and HCT116 proliferation, cells were treated with eight drug concentrations in a 96-well format and monitored for five days (Figure 6).

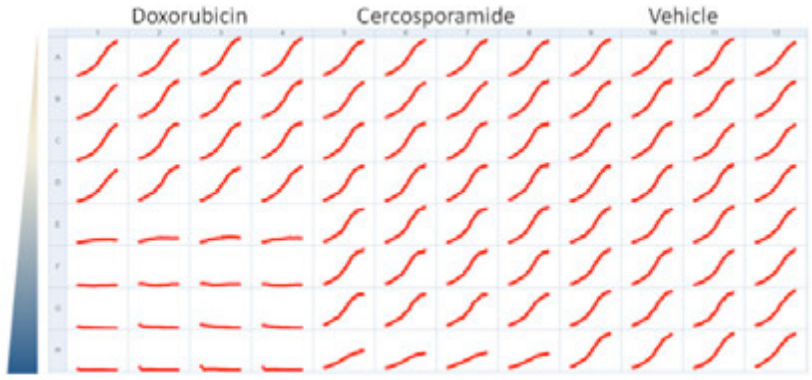

Figure 6. 96-well microplate matrix of HeLa cell proliferation over five days. Eight concentrations of doxorubicin and cercosporamide (4 replicates each) were tested alongside negative controls.

Kinetic cell proliferation profiles demonstrate the differential response to doxorubicin and cercosporamide across the three cell types (Figure 7).

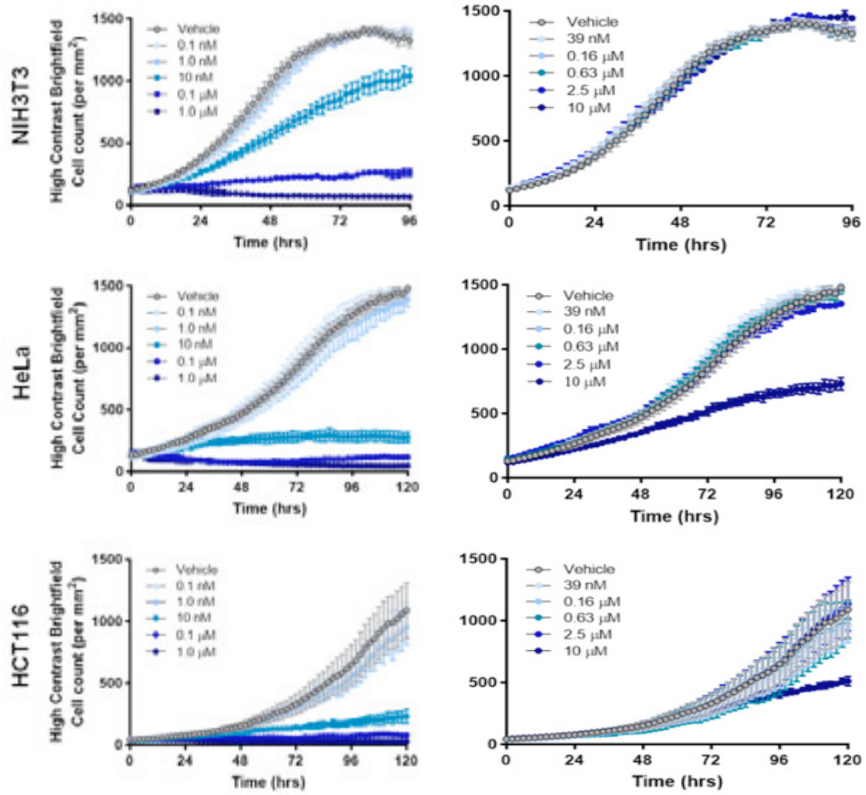

Figure 7. NIH3T3, HeLa and HCT116 cell proliferation profiles enable quantitative analysis of drug response. Cell counts per mm^2 were calculated every two hours for five days or until cells reached full confluence. Profiles from five drug concentrations demonstrate a cell type-dependent differential dose response.

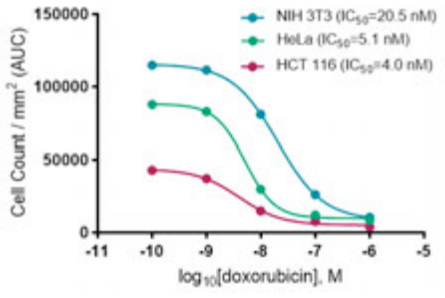

Figure 8. Measuring dose-dependent inhibition of cell proliferation by doxorubicin. AUC of cell count per mm^2 proliferation profiles were used to calculate IC_{50} values.

NIH3T3 cells were not affected by cercosporamide at any of the concentrations tested. However, proliferation of the two cancer cell types, HeLa and HCT116, was inhibited by 10 µM cercosporamide. Treatment with doxorubicin resulted in the dose-dependent inhibition of NIH3T3, HeLa and HCT116 cell proliferation. Quantitative analysis of the effect of doxorubicin treatment over time was provided by determining IC_{50} values using the area under the curve (AUC) from each proliferation profile (Figure 8). HCT116 had the highest sensitivity to doxorubicin, followed by HeLa and NIH3T3, with 4 nM, 5.1 nM, and 20.5 nM IC_{50} values, respectively.

Kinetic phenotypic analysis of cellular response to anti-proliferation drugs

To further examine the effects of doxorubicin treatment, experiment videos were used to conduct a qualitative evaluation of each cell type at inhibitory concentrations of the drug. A significant decrease in NIH3T3 cell numbers was observed within 36 hours at 10 nM doxorubicin, however no obvious signs of apoptosis were present. These findings indicate that at this concentration doxorubicin inhibits cell division without causing overt cytotoxicity. In contrast, NIH3T3 cells treated with 1 µM doxorubicin exhibited considerable cytotoxicity and signs of apoptosis within 24 hours (Figure 9).

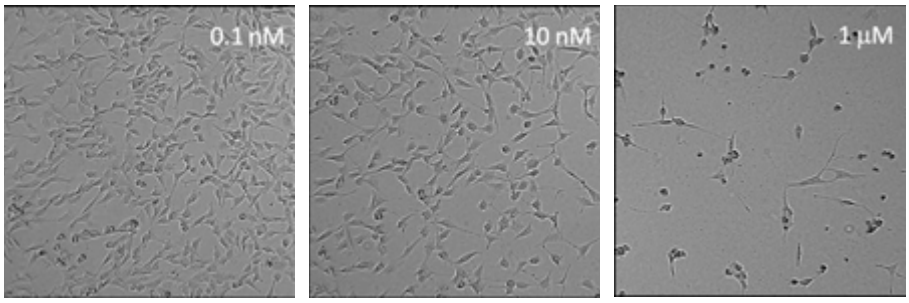

Figure 9. Qualitative analysis of kinetic cell proliferation provides valuable insight into phenotypic response to drug treatment. NIH3T3 proliferation images 36 hours after treatment with indicated concentration of doxorubicin. At 10 mM doxorubicin, cell division is inhibited without causing overt cytotoxicity. At 100 nM and higher, concentrations signs of cytotoxicity are evident.

Conclusion

Coupling the cell-handling abilities of the BioSpa 8 with the imaging capabilities of the Cytation 5 provides a fully automated system to conduct accurate and reproducible long-term proliferation studies. High-contrast brightfield cell counting enables quantitative analysis of cell growth without the need for disruptive labels. In addition to quantitative measures, this system can be used to conduct qualitative analysis of cell phenotypes over time, to further characterize drug treatment response or conduct targeted gene disruption studies. Proliferation assays can be run in 96- or 384-well microplates for medium- to high-throughput screening.

Together, the BioSpa 8 and Cytation 5, with the powerful Gen5 image analysis tools, provide an elegant and robust solution for a broad range of kinetic cell proliferation applications.

Recent publications using Agilent BioTek microscopes for label-free measurements of cell proliferation

1. M. A. Altemus et al., "Breast cancers utilize hypoxic glycogen stores via PYGB, the brain isoform of glycogen phosphorylase, to promote metastatic phenotypes," *PLOS ONE, vol. 14, no. 9, p. e0220973,* Sep. **2019**, doi: 10.1371/journal.pone.0220973.
2. A. C. Little et al., "IL-4/IL-13 Stimulated Macrophages Enhance Breast Cancer Invasion Via Rho-GTPase Regulation of Synergistic VEGF/CCL-18 Signaling," *Front. Oncol., vol. 9, p. 456,* May **2019**, doi: 10.3389/ fonc.2019.00456.

Figure 10. Typical tissue culture flasks with phenol red containing media.

Monitoring pH in long-term proliferation assays

Assay principle

Characterizing cell proliferation is a crucial aspect of biological research and therapeutic drug development. Most current cell proliferation assays rely on indirect biochemical metrics that are limited by artifacts or imaging-based end point measures. For example, DNA synthesis can be assessed though the incorporation of Thymidine analogs such as BrdU, EdU, and IdU. These analogs are then detected with specific antibodies or chemistries. Cellular metabolism can be assessed with tetrazolium salts that are converted to colored compounds by the action of cellular enzymes. Several different proliferation marker proteins, such as PCNA, Ki67and MCM-2 can be detected by immunofluorescence. While these technologies can provide a snapshot of cellular growth, they cannot necessarily provide information regarding long-term proliferation.

Long-term cellular *in vitro* proliferation assays have been shown to be extremely informative in regards to testing antiproliferative agents.[14] These assays take place over days in tissue culture media formulations intended to mimic nutrients normally supplied *in vivo*.

Most mammalian tissues exist at a near-neutral pH. Human arterial blood is maintained at 7.4 (7.35-7.45) by way of a bicarbonate buffer system regulated through normal body respiration. Deviations from the normal range induce the body to increase or decrease lung activity in order to alter CO_2 expiration.[15] Not surprisingly, *in vitro* cultivation of cells and tissues prosper at the same pH levels. Cultures are maintained at physiological pH primarily with a bicarbonatecarbonic acid buffer system as well. Bicarbonate-CO_2 systems use a matched concentration of dissolved bicarbonate with artificial levels of carbon dioxide gas. Carbon dioxide dissolves into the media forming carbonic acid as it reacts with water. Carbonic acid and bicarbonate also interact to form an equilibrium that is able to maintain pH at physiological levels.

Regardless of the buffering agent employed, tissue culture media is often supplemented with phenol red dye. While phenol red has been described as a weak estrogen under some conditions[16], it is for the most part an inert compound added to *in vitro* culture media as a visual pH indicator. While concentrations vary with different media formulations, when present, it is typically in the 5-15 mg/mL range.

Waste products produced by dying cells or overgrowth of contaminants will cause a decrease in pH, leading to a change in indicator color. For example, contamination of a culture of relatively slowly dividing mammalian cells can be quickly overgrown by bacteria, resulting in the acidification of the medium, and the indicator turning yellow. Mammalian cell waste products themselves will slowly decrease the pH, gradually turning the solution orange and then yellow. This color change is an indication that, even in the absence of contamination, the medium needs replacing.

Live cell imaging experiments focus entirely on the biology at hand. Whether the images are brightfield, phase contrast or fluorescent, the background milieu of the media is not observed and generally ignored. Here, we describe the use of the Cytation 5 cell imaging multimode reader to monitor cell culture pH status, while concurrently capturing digital microscopic images. This utilizes the unique capabilities of the reader to measure well absorbance in conjunction with cellular imaging.

Materials and methods

DMEM, Fetal Bovine Serum (FBS) and penicillin-streptomycin-glutamine were purchased from Life Technologies. Clear bottom, black sided 96-well microplates (3904) were from Corning.

Live cell experiments

HCT116-GFP colon cancer cells, expressing a nuclear H2B-GFP chimera fluorescent protein, were cultured in Advanced DMEM, supplemented with 10 % fetal bovine serum and penicillin-streptomycin at 37 °C in 5 % CO_2. Cultures were routinely trypsinized (0.05 % Trypsin-EDTA) at 80 % confluence. For experiments, cells were plated into Corning 3904 black sided clear bottom 96-well microplates. Long-term growth measurements were performed using a BioSpa 8 interfaced with a Cytation 5. The BioSpa system controls reader scheduling and maintains cells in a humidified controlled environment (37 °C, 5 % CO_2) in between imaging and plate absorbance measurements. As required, the BioSpa transports a microplate to the Cytation 5 for imaging and absorbance measurements and returns it to the incubator afterward. HCT116-GFP cells were seeded at either 500 or 2,000 cells per well. Cells were allowed to attach overnight before the initiation of growth measurements. HCT116-GFP cells were imaged using a Cytation 5 cell imaging multimode reader configured with a GFP light cube. The imager maintains 37 °C and 5 % CO_2 within the read chamber, and uses a combination of LED light sources in conjunction with band pass filters and dichroic mirrors to provide appropriate wavelength light. The GFP light cube consisting of a 469/35 excitation filter and a 525/39 emission filter for imaging cells expressing GFP. Montaged (2 x 2) digital images were made using a 4x objective and stitched into a single file using Gen5 microplate reader and imager software. Primary mask analysis of the captured digital images were used to determine the number of cells. Nuclei are identified as fluorescent objects between 5-100 µm in size and having fluorescence in excess of a threshold of 1,500. Immediately after imaging, the well absorbance at 560 nm was measured using the UV-Vis monochromator module of the Cytation 5.

Results and discussion

Live HCT116 cells expressing GFP in their nuclei are easily counted using image analysis. The green fluorescence identifies each cell without the need for a nucleic acid binding stain that could affect cell growth. When HCT116-GFP cells are seeded at low density and monitored over the course of five days, the 560 absorbance was used to calculate pH in each well by interpolating a previously determined pH calibration curve. The pH in these cultures decreased only about 0.15 over the course of five days, despite a 50-fold increase in the number of cells counted (Figure 11).

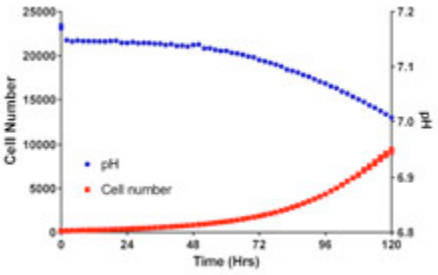

Figure 11. Change in HCT116 cell count and pH over time in nonconfluent cultures. HCT116 cells were seeded at a density of 500 cells per well. After 24 hours to allow for attachment, image-based and absorbance analysis were performed on 96-well plate cultures every two hours for five days and the results plotted. pH was determined by interpolating data from a previously generated calibration curve. Data represents the mean and SEM for 96 determinations at each data point.

In these experiments, cells were seeded at a density such that at the end of five days they have not reached confluence (Figure 12). In this state, the cells are not contact inhibited and can freely divide. The only limitations to division are media nutrients and media pH status.

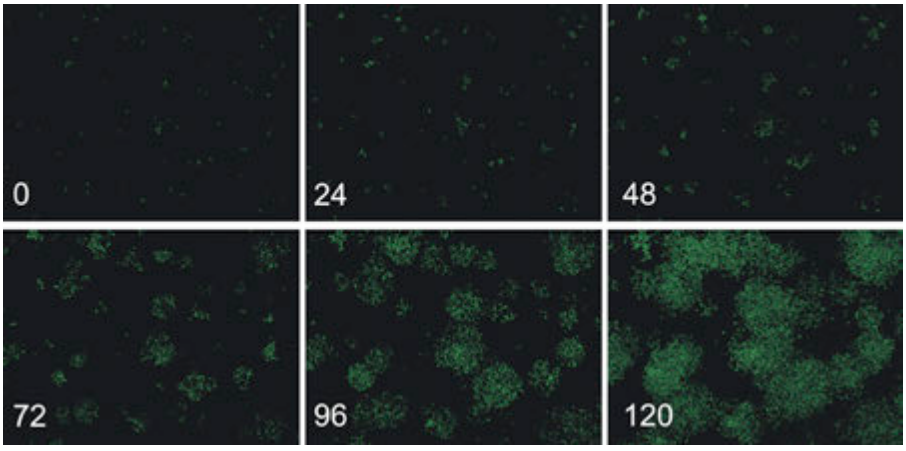

Figure 12. Montage images of HCT116-GFP cells in culture over five days. HCT116-GFP cells were seeded at 500 cells per well into a 96-well plate and allowed to attach for 24 hours. Montage-images (2 x 2) were made with a 4x objective every 24 hours using a GFP LED cube.

This is corroborated with a comparison of the cell number to the 415/560 absorbance ratio. This ratio is a function of the color of the media, which we have shown previously to be inversely related to its pH.[17] As seen in Figure 13, the cell number increases with time in these cell cultures. Under these conditions, cells are able to grow and divide unimpeded, and with time the determined cell number increases. Individual well cell numbers may vary due to variations in the physical location of the cells, as well as differences in initial cell number. Because the stitched image used for cell counting only encompasses the center portion of the well, cells attached around the perimeter of the well would not necessarily be counted. Likewise, wells that receive slightly more or slightly fewer cells with the initial seeding would be expected to have different cell counts at later time intervals. Despite the variability in cell count, cell numbers increase in a linear fashion over time. With time and increases in cell number, wells have a lower pH.

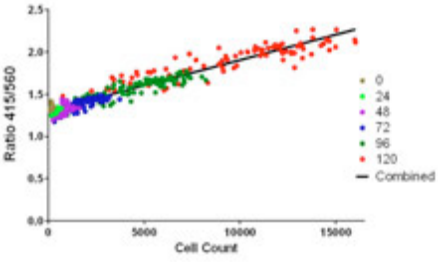

Figure 13. Relationship between media coloration and cell number at low cell density seeding. Cell counts for each well of a 96-well plate cultured over a 5-day period plotted against the 415/560 absorbance ratio. Each data point represents an individual well.

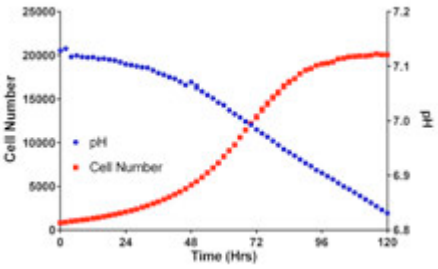

Figure 14. Change in HCT116 cell count and pH over time in confluent cultures. HCT116 cells were seeded at a density of 2,000 cells per well. After 24 hours to allow for attachment, image-basedand absorbance analysis performed on 96-well plate cultures every two hours for five days. pH was determined by interpolating the 415/560 ratio values with a previously generated calibration curve. Data represents the mean and SEM for 96 determinations at each data point.

When HCT116-GFP cells are seeded at higher density, pH change becomes a greater issue and cell number increase eventually stalls (Figure 14). When cells are seeded at 2,000 cells per well, the increased number of cells causes the pH to drop about 2-fold more than the lower seeding density. This drop in pH continues the length of the experiment despite the cell number stalling after about 80 hours. At higher cell densities, cell continues throughout the length to respire, despite the cessation of cell number increase, resulting in a decrease in the pH.

The cellular confluence can be seen in Figure 15, where there is little increase in the fluorescence observed between hour 96 and hour 120.

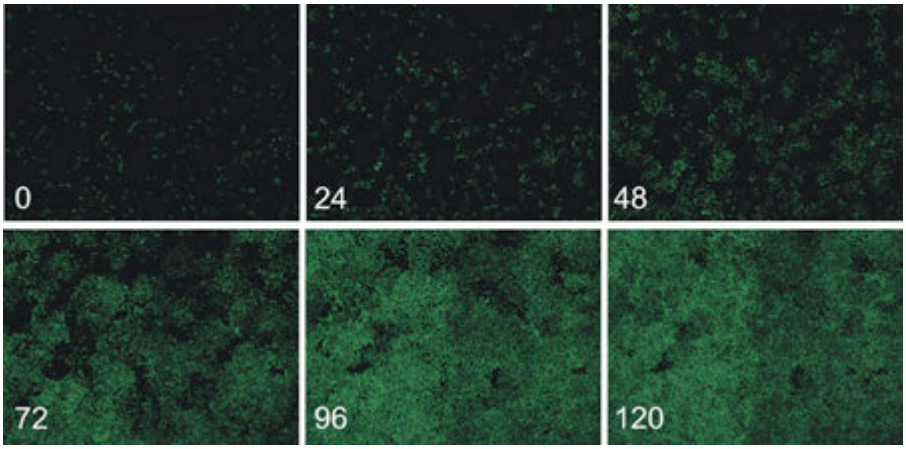

Figure 15. Montage images of HCT116-GFP cells in culture over five days. HCT116-GFP cells were seeded at 2,000 cells per well into a 96-well plate and allowed to attach for 24 hours. Montage-images (2 x 2) were made with a 4x objective every 24 hours using a GFP LED cube.

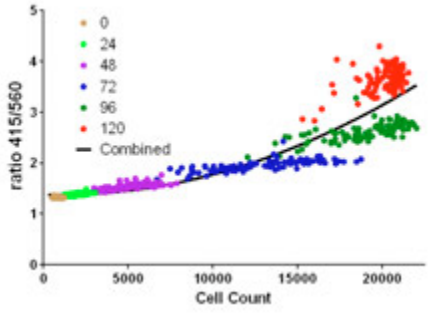

Figure 16. Relationship between media coloration and cell number at high cell density seeding. Cell counts for each well of a 96-well plate cultured over a 5-day period plotted against the 415/560 absorbance ratio. Each data point represents an individual well.

The inhibition of growth as a result of cellular confluence in long-term cultures can be identified with cell counting. As observed in Figure 16, cell number, as determined from image-based counting of nuclei, no longer increases with time as cells become confluent. The cell number after four or five days does not increase appreciably. However, the pH of the media present does decrease as observed by an increases in the 415/560 absorbance ratio. Despite little to no increase in cell numbers, waste products continue to be excreted and nutrients are consumed by the cells present.

These data demonstrate that the Cytation 5 is capable of monitoring cell culture pH in live cell experiments while concurrently imaging. Cell cultures normally become acidic due to an increase in cell numbers and cellular respiration, resulting in a yellowing in color of media formulations containing phenol red. While the change in pH for short-term experiments is often negligible, with long-term live cell experiments increasing cell numbers and the longer duration can overwhelm the buffering capacity of the media formulation. The ability to monitor changes in culture pH in real time can allow the researcher to have confidence in the observed experimental results or abort experiments that have deleterious pH conditions.

Monitoring cell numbers or cell confluency over time is commonly used to test the efficacy of antineoplastic agents in preventing cell growth. The use of phenol red absorbance to monitor media pH ensures that reported inhibition is the result of the test compound rather than poor tissue culture media status.

The Cytation 5 is an ideal platform to monitor phenol red absorbance change with live cell imaging experiments. The reader is unique in that it has the capabilities of both the absorbance measurements using a dedicated UV-vis monochromator and microscopic imaging using a 6-position objective turret and LED light cubes. The rapid speed of the absorbance reading adds only seconds to a full 96-well imaging step, but can provide effective information regarding cell culture status. In addition to controlling reader function, the Gen5 can be used to calculate pH from previously established pH calibration curves. This unique combination allows continual real-time monitoring of long-term live cell culture experiments.

Fluorescent markers in proliferation assays

By using fluorescent markers, additional details of the cellular death state like apoptosis and necrosis can be measured. Additionally, labeled cell counts give excellent results on a variety of cell types where label-free counting isn't necessary.

Automated kinetic imaging assay of cell proliferation in 384-well format

Assay principle

Even from the beginning of life, the proper function of all multicellular organisms depends on cell death. Mismanaged cell death underlies phenomena ranging from developmental abnormalities to cancer. The ability of cancerous cells to evade regulated cell death, or apoptosis, is particularly problematic for cancer treatment.[18] Whether through radiation, immunotherapy or chemotherapy, the goal of cancer treatment is the selective death of the cancerous cells. Understanding the many facets of cell death, and in particular those aspects that cancer cells are able to overcome, is an active area of interest for clinicians, primary researchers and drug discovery efforts alike.[18] Imaging-based tools to monitor cells undergoing different cell death mechanisms have provided a means to probe cell death in a continuous, live, high-throughput manner.

Regulated cell death, such as apoptosis, and accidental cell death, such as necrosis, are both processes that can occur in response to a cellular stressor (ie. nutrient deprivation or DNA damage), but each produce different hallmark cellular changes.[19] One of the characteristics of early state apoptosis occurs when phosphatidylserine, a membrane component normally only found within the inner leaflet of cell membranes, translocates to the outer leaflet. This exposure of phosphatidylserine likely prompts engulfment of the cell, or remaining cell fragments, by phagocytes.[20] Here, we optically monitor

phosphatidylserine exposure in live cells through its specific binding and activation of the fluorescent pSIVA-IANBD probe. This fluorescent probe provides a live, kinetic indicator of cells undergoing apoptosis and persists through cell death.[21]

A characteristic change during both late-stage apoptosis and necrosis processes is that cell membrane integrity is lost.[19] This loss of integrity allows molecules to enter cell nuclei that are normally excluded, such as the DNA staining dye propidium iodide (PI). Therefore, fluorescent PI staining of nuclei can also be monitored in real-time as a measure of cells undergoing necrosis and late-stage apoptosis processes.

Here, we have combined long-term kinetic label-free cell counting and fluorescent imaging to monitor cancer cell responses over several days in a high-throughput 384-well image-based assay. The Cytation 5 with wide-field-of-view camera enables capture of the entire 384-well in a single image. Coupling the Cytation 5 with the BioSpa for fully automated environmental control allows for a walk-away workflow of high-throughput image-based cellular analysis.

Materials and methods

Reagents

HT-1080 fibrosarcoma cells were obtained from ATCC (Manassas, VA). Advanced DMEM, Fluorobright DMEM, fetal bovine serum (FBS), and glutamine/penicillin/streptomycin were purchased from Thermo Fisher Scientific (Waltham, MA). Staurosporine, nocodazole, nigericin and camptothecin were purchased from Tocris Bioscience (Minneapolis, MN). The Kinetic Apoptosis Kit for microscopy (ab129817) was purchased from Abcam (Cambridge, MA). Greiner 384-well microplates (Cat. No. 781091) were obtained from Sigma-Aldrich (St. Louis, MO).

Cell culture and assay preparation

HT-1080 cells were maintained in Advanced DMEM media supplemented with 10 % FBS, 2 mM glutamine and penicillin/streptomycin at 37 °C in a humidified incubator with 5 % CO_2. Cells were routinely passaged at 80 % confluency. For seeding in 384-well microplates, HT-1080 cells were harvested and suspensions were added at a density of 500 cells per well. After cells adhered (approximately four hours), media was exchanged for Fluorobrite DMEM media. The Kinetic Apoptosis Kit reagents were added to each well to a final concentration of 1 µL/mL pSIVA-IANBD and 2 µL/mL PI. Dilution series of antineoplastic drugs were added across the microplate, and imaging was started immediately following drug addition.

Automated long-term live cell imaging

For fully automated long-term imaging, cells were maintained in a BioSpa 8 coupled to a Cytation 5 with wide-field-of-view camera. The BioSpa 8 maintained cells at 37 °C, 5 % CO_2 and 80-90 % humidity throughout the course of the 72-hour experiment, and environmental parameters were monitored and reported live

through the BioSpa software. The microplate was automatically transferred from the BioSpa incubator to the Cytation 5 at two-hour intervals for imaging. Additional environmental controls inside the Cytation 5 maintained cells at 37 °C and 5 % CO_2 throughout the imaging procedure.

Single-image whole-well capture

For whole-well imaging of the 384-well microplate, the Cytation 5 with wide-field-of-view camera was paired with a 4x magnification objective. The Cytation 5 wide-field-of-view enabled a single-image capture of the entire culture area of the well (Figure 17). The Cytation 5 was configured for imaging as shown in Table 2. Imaging cubes GFP (469/525 nm) and PI (531/647 nm) were used for detection of Kinetic Apoptosis Kit reagents pSIVA and PI signals, respectively. For label-free cell counting, the Cytation 5 with High Contrast Brightfield Kit was used as described previously.[14]

Table 2. Agilent BioTek Gen5 microplate reader and imager software settings for image acquisition.

Image Acquisition	
Parameter	**Value**
Channel	Brightfield (high-contrast)
	GFP 469,525
	Propidium iodide 531,647
Focus	Laser autofocus
Objective	4x PL FL
Z-stack	No
Montage	No
Discontinuous Kinetic Procedure	Yes
Estimated Total Time	3 days
Estimated Interval	2 hours

Image analysis

FImage processing was performed using Gen5 software. The parameters used are listed in Table 3. Preprocessing reduced background and enhanced contrast, readily enabling cell identification in all channels. For the high-contrast brightfield image, processing results in an image with a black background, and bright white spots corresponding to cells.

Table 3. Agilent BioTek Gen5 microplate reader and imager software image processing parameters.

Image Processing			
Parameter	**Brightfield**	**GFP 469,525**	**Propidium Iodide 531,647**
Background	Dark	Dark	Dark
Rolling Ball Diameter	20	100	30
Priority	Fine results	Fine results	Fine results
Image Smoothing Strength	5 cycles	1 cycle	1 cycle

Cellular analysis was performed on preprocessed images and the parameters for all channels used are listed in Table 4. For each channel, the threshold value was determined through the image statistics analysis in Gen5. Image statistics of control wells was carried out, and three standard deviations above the average image signal was used as the threshold value for cellular analysis. Total cell counts were established through primary mask analysis of the high-contrast brightfield image. The number of cells positive for the apoptotic reporter pSIVA was established through primary mask analysis of the GFP channel. The number of cells positive for the necrotic marker, PI was established through primary mask analysis of the PI channel. The liquid meniscus introduced an imaging artifact where the corners of the square well were slightly less illuminated in brightfield than the rest of the culture area (Figure 17), potentially introducing bias in the label-free cell counts compared to fluorescence counts. The Gen5 plug feature was used to restrict cellular analysis to the area of the well best illuminated in brightfield (a 3,400 µm diameter circle), corresponding to ~92 % of the total well culture area. Therefore the plug feature enabled unbiased normalization of fluorescent cell counts using label-free cell counting methods.

Table 4. Agilent BioTek Gen5 microplate reader and imager software cellular analysis parameters.

Cellular Analysis			
Primary Mask			
Parameter	**Brightfield Cell Count**	**pSIVA Count**	**PI Count**
Detection Channel	Tsf[Brightfield]	Tsf[GFP 469,525]	Tsf[Propidium iodide 531,647]
Threshold	8,000	4,000	3,000
Background	Dark	Dark	Dark
Split Touching Objects	Yes	Yes	Yes
Fill Holes in Masks	Yes	Yes	Yes
Minimum Object Size	10 µm	15 µm	5 µm
Maximum Object Size	100 µm	100 µm	100 µm
Include Primary Edge Objects	No	No	No
Analyze Entire Image	No	No	No
Advanced Detection Options			
Rolling Ball Diameter	Auto	50	30
Image Smoothing Strength	3 cycles	3 cycles	3 cycles
Evaluate Background On	5 %	5 %	5 %
Primary Mask	Use threshold mask	Use threshold mask	Use threshold mask

Curve fitting and statistics

All data was collected and analyzed using Gen5 software. For data presentation, both Gen5 and GraphPad Prism V8 software were used. All curve fitting and EC_{50} analysis was performed in Gen5. Time of V_{max} analysis in Gen5 was performed over a 5-point window for linear regression. Statistical analysis for was performed using the Student's t-test function (two-tailed, unpaired) in Microsoft Excel.

Results and discussion

Automated kinetic analysis of proliferation

Label-free image-based cell counting of the human fibrosarcoma cell line HT-1080 was performed at two-hour intervals over three days in a 384-well plate. For each well, a single image was captured using a 4x objective and the High Contrast Brightfield Kit. Cell counts were established using cellular analysis in Gen5 (Figure 17).

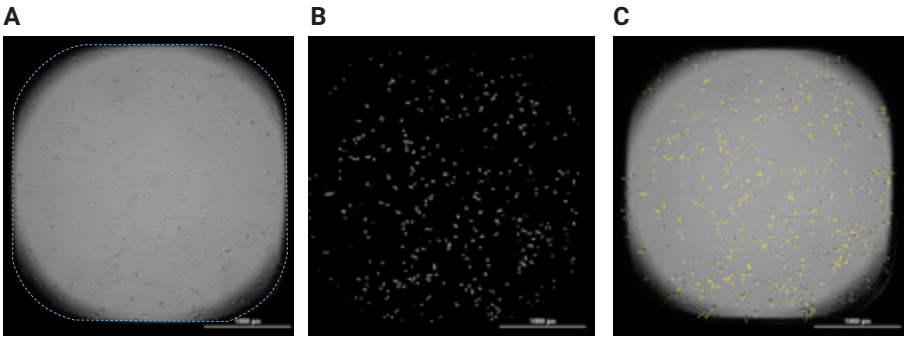

Figure 17. Label-free high-contrast cell counting method. (A) Original high-contrast defocused image captured with the High Contrast Brightfield Kit. Total culture area of a single well of the 384-well plate is outlined by the dashed blue line. (B) High-contrast brightfield image after preprocessing steps indicated in table 3. (C) Agilent BioTek Gen5 microplate reader and imager software cellular analysis identifies and counts HT-1080 cells (yellow), shown overlaid on original high-contrast brightfield image.

The effect on cell proliferation of four antineoplastic drugs, staurosporine, nocodazole, camptothecin and nigericin was examined. The drugs were added just before the first images were acquired at t=0 hours. Gen5 software generated curves of cell counts providing a visual overview of proliferation rates for the entire 384-well dish (Figure 18). The differential inhibitory effect of each drug on proliferation was readily appreciated in the Gen5 plate overview.

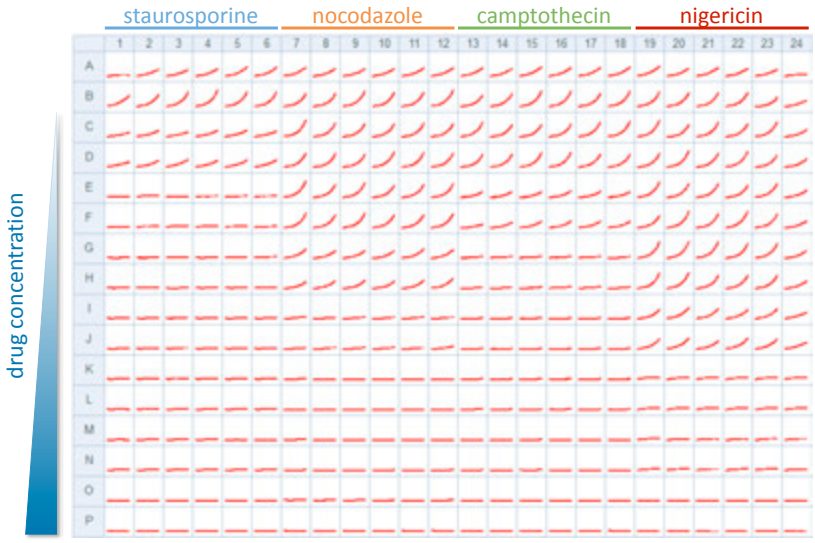

Figure 18. 384-well plate overview of cell proliferation. Red curves indicate cell count plotted over the duration of the three day experiment. As drug concentration increases from rows C through P, reduced proliferation is observed for all drugs across the entire 384-well plate.

For two example drugs, nocodazole and camptothecin, cell counts are plotted together across the different doses (Figure 19A, 19B). For all further analysis, replicates of 12 wells for each condition were averaged and plotted together. To quantify the inhibitory effect of each drug on proliferation, dose-response curves were generated in Gen5 (Figure 19C, 19D). Dose-response curves were first generated for different drugs through single time point analysis at 24 hours.

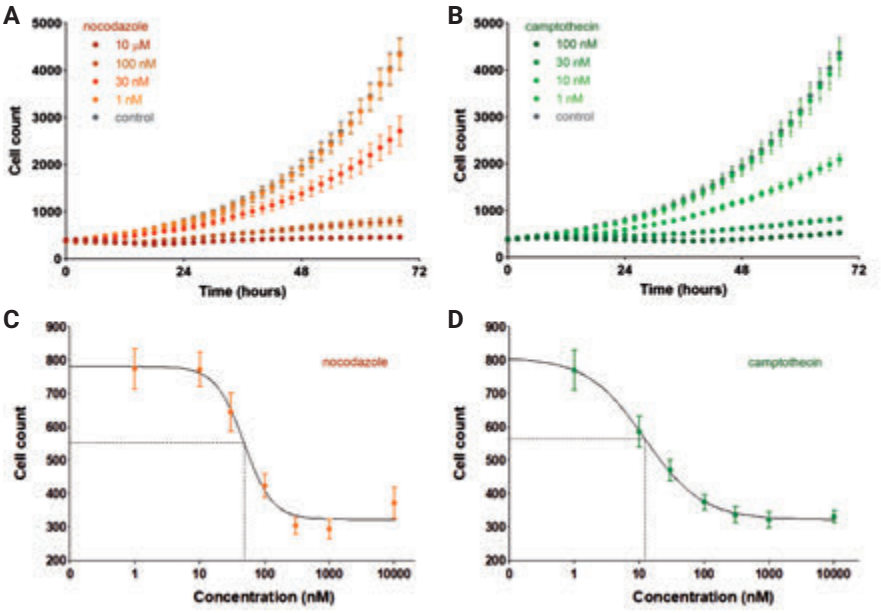

Figure 19. Dose-dependent inhibition of HT-1080 fibrosarcoma cell proliferation. Average cell count plots are overlaid for several concentrations of (A) nocodazole (orange circles, n=12 replicate wells) and (B) camptothecin (green circles, n=12 replicate wells) over three days. Error bars indicate standard deviation of replicates. Agilent BioTek Gen5 microplate reader and imager software generated dose-response curves for label-free cell counts at a single time point of 24 hours for (C) nocodazole (orange circles) and (D) camptothecin (green circles). The 4-parameter fits are indicated in black solid lines, and interpolated IC_{50} values are visualized with dashed lines. For nododazole, the IC_{50} corresponds to 48 nM, and for camptothecin corresponds to 12 nM.

Gen5 provides an additional comparison of IC_{50} values from integral analysis of the area under the curve (Figure 20). This way of calculating IC_{50} values was independent of drug exposure time, and accounted for changes across the duration of the experiment. For camptothecin, IC_{50} values were in good agreement between analysis methodologies. For comparison, AUC analysis was also done for nigericin and nocodozole, demonstrating assay sensitivity across large variations in IC_{50} (Figure 20C).

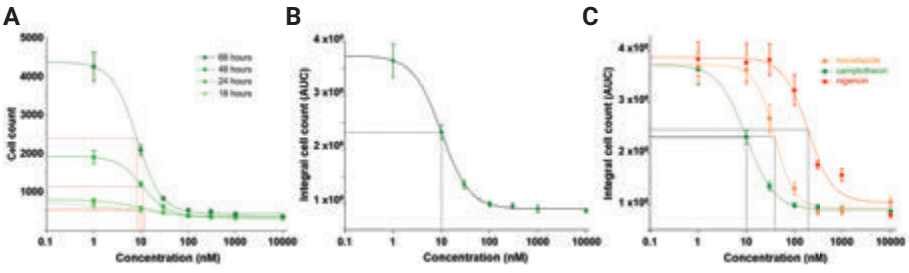

Figure 20. Label-free proliferation dose-response curves with IC_{50} analysis. (A) Dose-response curves for multiple time points are overlaid for camptothecin, allowing time-dependent comparison of IC_{50} values (18 hours = 9.5 nM, 24 hours = 12.3 nM, 48 hours = 10.9 nM, and 68 hours = 8.2 nM). For each curve the 4-parameter fit is colored and the IC_{50} interpolation is visualized in dashed lines. (B) Agilent BioTek Gen5 microplate reader and imager software provides additional estimates of IC_{50} values through area-under-the-curve (integral) analysis for the entire kinetic series (IC_{50} = 10 nM). (C) Integral-based dose-response curves for three drugs indicated. Solid lines correspond to 4-parameter fit, and dashed lines indicate IC_{50} interpolation. IC_{50} values correspond to 10 nM for camptothecin, 39 nM for nocodazole, and 193 nM for nigericin.

Fluorescence-based kinetic cell death phenotype

In addition to the overall effect on proliferation, the mechanism of cell death was examined using fluorescent reporters of apoptosis and necrosis. At each time point where brightfield images were taken, corresponding fluorescence images were taken of the apoptosis marker pSIVA and the necrosis marker PI (Figure 21A). Cells were identified positive for pSIVA and PI signals (Figure 21B, see "Materials and methods" for identification parameters) and primary masks identified individual cells for each well and time point (Figure 21B, see inset).

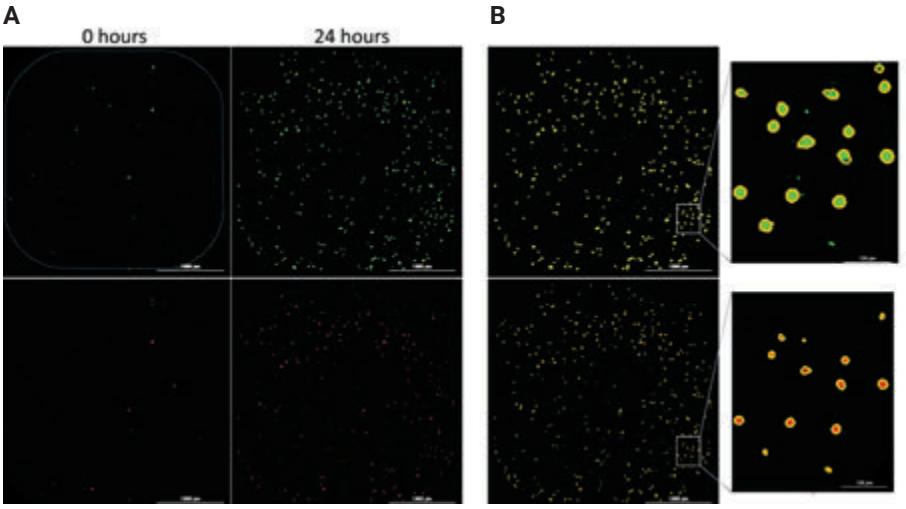

Figure 21. Capture and identification of cells positive for apoptosis and necrosis. (A) Example images of cells positive for pSIVA apoptosis marker (green, upper panels) and PI necrosis marker (red, lower panels) at two time points (indicated). The area of the 384-well bottom is indicated by the dashed blue outline in the top left panel of A. (B) Positive apoptotic and necrotic cells were identified by size and signal threshold parameters (see "Materials and methods") and primary masks identified positive cells (inset shows enlarged region for clarity).

Quantitative analysis of apoptosis

The green fluorescence of pSIVA will increase as phosphotidylserine is exposed to the extracellular space. As expected, the number of cells positive for the apoptosis marker pSIVA increases over time in response to antineoplastics, but remains relatively stable at a low level in control wells (Figure 22A). Although the behavior is expected at the highest and lowest concentrations of nocodazole, at intermediate concentrations the number of cells positive for pSIVA continues to increase over time. This accumulation is due to the continued proliferation of the total cell population, despite that many of the cells actively undergoing cell death. This effect obscures the interpretation of the results, as well as left-shifts the EC_{50} value of the resultant dose-response curve over time (Figure 22A, bottom panel).

To control for the continued proliferation of the cells, as well as any initial variability in cell numbers between conditions and replicates, the pSIVA positive cell counts can be expressed as a percent of total cell counts established through the label-free cell counts (Figure 22B). Importantly, normalizing apoptotic counts to total cell counts demonstrates that the percent of apoptotic cells remains

stable at a given drug concentration, despite absolute increases in both label-free cell counts and pSIVA positive counts (Figure 22B, top panel). Furthermore, EC_{50} values at different time points are stable over time, and nearly identical for normalized counts (Figure 22B, bottom panel). Therefore, quantification of the apoptotic fluorescence signal based solely on absolute counts systematically and substantially underestimates the EC_{50} value over time when cells at intermediate drug concentrations continue to proliferate.

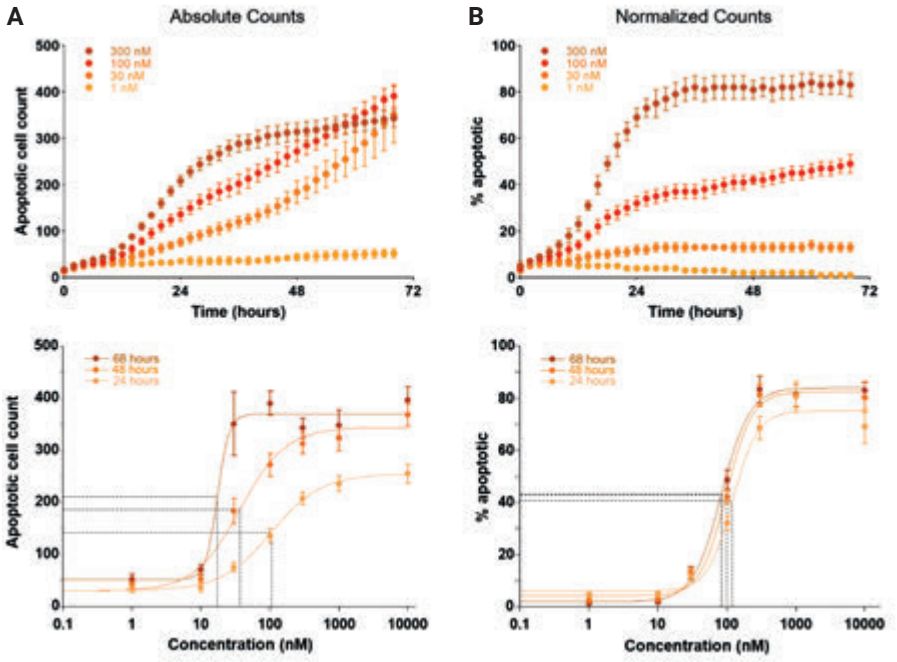

Figure 22. Apoptotic signal response to antineoplastics. (A) Apoptotic cell counts for the drug nocodazole applied at the four concentrations indicated. Note that apoptotic cell counts continue to rise for intermediate concentrations due to total cell counts increasing. For absolute cell counts, dose-response curves were generated and fit to the three time points indicated. EC_{50} values were substantially left-shifted over time due to cell proliferation (EC_{50} 24 hours = 106 nM, EC_{50} 48 hours = 30 nM, EC_{50} 68 hours = 17 nM). (B) The same data for apoptotic cell counts from panel A, but normalized to total cell counts (expressed as percent). For normalized apoptotic cells, all dose-response curves consistently resulted in an EC_{50} value of approximately 100 nM. For both A and B lower panels, Agilent BioTek Gen5 microplate reader and imager software 4-parameter fit lines are shown in solid colors, and EC_{50} interpolation lines are shown as dashed.

Quantitative analysis of necrosis

Additionally, the Kinetic Apoptosis Kit includes propidium iodide (PI) as a reporter of necrosis and late apoptosis. PI enters the cell and intercalates DNA when both the cellular and nuclear membranes are compromised; membrane integrity is lost both during late apoptosis and necrosis processes. Here, PI binding is monitored and quantified through fluorescence imaging. As with the pSIVA signal, PI signals generally increase over time and with increased drug dosage, as shown for nocodazole (Figure 23A). As is also seen with the pSIVA apoptosis signal, the PI positive cells also increases at intermediate drug concentrations due to proliferation. Therefore, PI positive cells were also normalized as a percent of total cells using label-free cell counts (Figure 23B).

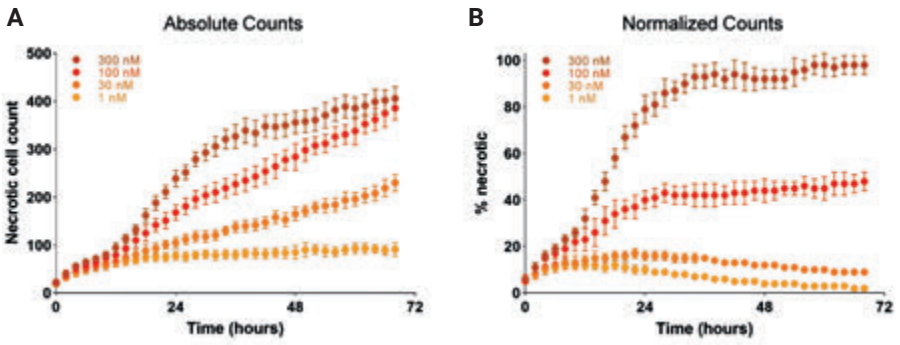

Figure 23. Necrotic signal response to antineoplastics. (A) Necrotic cell counts for the drug nocodazole applied at the four concentrations indicated. Note that necrotic cell counts continue to rise for intermediate concentrations due to total cell counts increasing. (B) The same data for apoptotic cell counts from panel A, but normalized to total cell counts (expressed as percent).

For comparison and quantitation of drug efficacy, kinetic analysis and curve fitting was performed for normalized necrosis and apoptosis signals for all drugs at 24 hours (Figure 24). Interestingly, despite nigericin's efficacy in inhibiting proliferation (IC_{50} = 100 nM, Figure 20C), it resulted in little apoptosis or necrosis at even the highest concentrations used, and EC_{50} values for apoptosis and necrosis were undetermined.

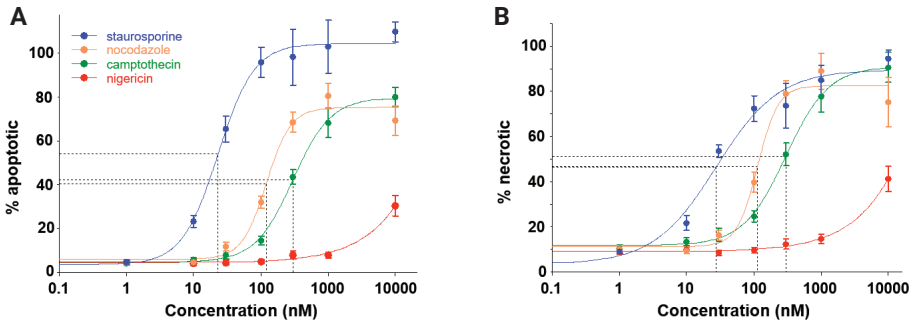

Figure 24. EC_{50} determination for apoptosis and necrosis. Dose-response curves for percent necrotic (left panel) and percent apoptotic cells plotted for each drug indicated. Agilent BioTek Gen5 microplate reader and imager software 4-parameter fits are shown for each fit (solid colored lines) as well as interpolated EC_{50} values (dashed lines). For apoptosis, EC_{50} values correspond to 24 nM for staurosporine, 121 nM for nocodazole and 301 nM for camptothecin. For necrosis, EC_{50} values correspond to 28 nM for staurosporine, 114 nM for nocodazole, and 301 nM for camptothecin. EC_{50} values for nigericin (red) were undetermined for both apoptosis and necrosis.

Additionally, the maximal plateau values for staurosporine reached higher levels for percent apoptosis, compared to percent necrosis, despite similarities in the EC_{50} values for both processes. This difference potentially indicates that staurosporine preferentially initiates apoptosis in HT-1080 cells. Therefore, quantitative investigation into the onset time of the apoptosis and necrosis

signals was also performed using Gen5. In Figure 25A, traces of percent apoptosis and percent necrosis are both shown for staurosporine (blue) and camptothecin (green). By eye, for cells treated with staurosporine the apoptosis signal precedes the necrosis signal. For comparison, the percent apoptosis and necrosis signals onset times are nearly identical for camptothecin, as both traces overlap significantly. To quantify this difference, the time of V_{max} parameter was measured for each trace (see "Materials and methods" for details). To evaluate time of V_{max} for each drug, the first concentration approaching maximal levels of percent apoptosis and necrosis was chosen. The time of V_{max} for each drug is shown in Figure 25B. Only staurosporine showed an onset time difference between the two signals, with apoptosis proceeding necrosis by ~3.5 hours. This finding indicates that the mechanism of cell death is primarily through apoptosis, leading to necrosis.

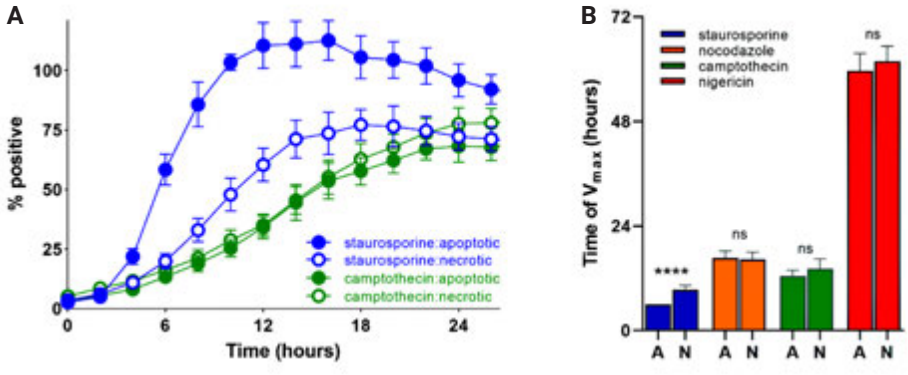

Figure 25. Onset time comparison for apoptosis and necrosis processes. (A) Example traces for apoptosis signal (filled circles) and necrosis signal (open circles) plotted together for the same cell population. For staurosporine (blue traces), but not camptothecin (green traces), apoptosis proceeds necrosis signals. (B) Plot comparing time of V_{max} parameter for apoptosis (abbreviated as "A") and necrosis (abbreviated as "N"). Only staurosporine showed a significant (p=0.000001) difference between time of $V_{max,}$ with apoptosis occurring ~3.5 hours earlier than necrosis.

The Cytation 5 with wide-field-of-view camera paired with the BioSpa 8 automated incubator provides a fully automated and robust means of quantifying image-based assays of cell proliferation and cell death. The wide-field-of-view camera allows single image capture of whole-well culture area, minimizing image capture time and improving compatibility for small culture area vessels for high-throughput applications. Gen5 software and cell analysis routines allow for quick, automated identification of cell counts, for both brightfield and fluorescence-based images. Normalization of fluorescence signals using the label-free cell counts was critical to avoid bias in EC_{50} determination due to differences in proliferation rates between conditions.

Utilizing automated, multiparametric methods to quantify kinetic cell death analyses

Assay principle

Deep insight into regulation and dysregulation of cell death processes is critical towards understanding disease states such as cancer, and developing effective, well-tolerated treatment therapies. In fact, many programmed and non-programmed cell death pathways are being studied to develop more effective and less toxic chemotherapeutic regimens.[22] However, the diversity of cell death modalities is complicated by shared signaling elements, overlapping mechanisms, and complex crosstalk among various cell death pathways.[23] Differentiating the morphological hallmarks of cell death pathways can be labor intensive, and when incorporating end point assays, can often miss critical yet transient events.

Here, we demonstrate an automated, multiplexed method to assess real-time cell death using a live cell imaging system. Three common cell death biomarkers are measured: mitochondria membrane potential, phosphatidylserine (PS) externalization, and cell membrane integrity, using fluorescent probes from Abcam. The fluorescent, positively-charged tetramethylrhodamine ethyl ester (TMRE) dye readily passes through cell membranes and accumulates in healthy, active mitochondria, where it produces a red-orange signal. If the mitochondria membrane is depolarized or inactive, as in apoptotic and necrotic cells, the dye diffuses throughout the cell. The green fluorescent probe, pSIVA-IANBD binds to the non-polar environment of the cell's membrane lipid bilayer, and detects irreversible and transient phosphatidylserine exposure that is characteristic of apoptosis and necroptosis. Finally, the far-red fluorescent dye, DRAQ7 is impermeant in healthy cells, while it stains nuclei in dead and permeabilized necrotic and necroptotic cells. Combining these dyes into a single, multiplexed method with real-time morphological analysis provides major advantages when characterizing cell death systems. Fibrosarcoma target cells and dyes were combined in a microplate along with a known inhibitor compound, and incubated in an automated benchtop incubator. The plates were automatically transferred from the incubator to a combined microplate reader and automated digital imager every two hours for a total of 48 hours, where fluorescent imaging was performed to assess cellular activity, as well as high-contrast brightfield imaging to allow for accurate cell counting over the entire incubation period.

Materials and methods

Cells and media

HT-1080 fibrosarcoma cells (part number CCL-121) were obtained from ATCC, Manassas, VA. Advanced DMEM (part number 12491-015), fetal bovine serum, (part number 10437-036), and penicillin-streptomycin-glutamine (100X) (part number 10378-016) were purchased from Thermo Fisher Scientific (Waltham, MA).

Assay and experimental components

The TMRE fluorescent dye, as part of the TMRE-Mitochondrial Membrane Potential Assay Kit (part number ab113852), pSIVA-IANDB green fluorescent probe, as part of the Kinetic Apoptosis Kit (part number ab129817), DRAQ7 far-red fluorescent dye (part number ab109202), and the known topoisomerase I inhibitor, camptothecin (part number ab120115) were provided by Abcam (Cambridge, MA).

Cell preparation

A total of 2000 HT-1080 fibrosarcoma cells in prepared media were added to wells of a 96-well tissue culture-treated microplate. The microplate was incubated at 37 °C/5 % CO_2 overnight to allow the cells to attach to the wells.

Reagent and inhibitor dilutions

Assay reagents were diluted in media to the following 1x working concentrations: 200 nM TMRE; 10 µL/mL pSIVAIANDB; 3 µM DRAQ7. Camptothecin was diluted in media containing reagents to create an eight-point titration from 10 µM to 0 µM using serial 1:4 dilutions.

Assay procedure

Following overnight cell attachment, media was removed from the microplate and replaced with media containing the TMRE, pSIVA, and DRAQ7 reagents in addition to compound dilutions. The plate was then placed into the BioSpa 8, with atmospheric conditions previously set to 37 °C/5 % CO_2. Water was added to the pan to create a humidified environment. The BioSpa 8 software was programmed such that the plates were automatically transferred to Cytation 5 for high-contrast brightfield and fluorescent imaging of the test wells every two hours for a total of 25 imaging iterations over the 48-hour incubation period. A single 4x image was taken with each channel (Table 5) to capture a representative population of cells per well. Laser autofocus was incorporated to ensure proper focusing on the target cell layer as well as the most efficient focusing procedure.

Table 5. Cells imaged per channel.

	Imaging Channel Target
HCBF	All cells
GFP	Apoptotic cells
RFP	Active mitochondrial membrane potential
CY5	Necrotic cells

Image processing

Following capture, images were processed prior to analysis to remove background signal from each channel using the settings in Table 6.

Table 6. Image preprocessing parameters.

2D Image Preprocessing Parameters			
Channel	**Apply Image Preprocessing**	**Background**	**Rolling Ball Diameter**
HCBF	Yes	Dark	25
GFP	Yes	Dark	Auto
RFP	Yes	Dark	150 µm
CY5	Yes	Dark	Auto

Cellular analysis of processed images

Cellular analysis was carried out on the processed images to determine the total cell number per image, in addition to the cell number meeting the criteria for active mitochondria, apoptotic, and necrotic activity using the criteria in Tables 7 and 8.

Table 7. Primary and secondary analysis criteria.

Total Cell Primary Analysis	
Channel	Tsf[Brightfield]
Threshold	10,000
Background	Dark
Split Touching Objects	Checked
Fill Holes in Masks	Checked
Minimum Object Size	5 µm
Maximum Object Size	100 µm
Include Primary Edge Objects	Unchecked
Analyze Entire Image	Checked
Advanced Detection Options	
Rolling Ball Diameter	25 µm
Image Smoothing Strength	0
Evaluate Background On	5 % of lowest pixels
Active Mitochondria Cell Secondary Analysis	
Channel	Tsf[RFP]
Measure Within a Secondary Mask	Checked
Type	Exclude primary mask
Distance from Primary Mask	1 µm
Ring Width	25 µm
Threshold	5,000
Smoothing	0
Method	Propagate mask
Metric of Interest	Area_2[Tsf[RFP]]
Apoptotic Cell Secondary Analysis	
Channel	Tsf[GFP]
Measure Within a Secondary Mask	Checked
Type	Exclude primary mask
Distance from Primary Mask	1 µm
Ring Width	25 µm
Threshold	10,000
Smoothing	0
Method	Propagate mask
Metric of Interest	Mean_2[Tsf[GFP]]
Necrotic Cell Secondary Analysis	
Channel	Tsf[CY5]
Measure Within a Primary Mask	Checked
Expand Primary Mask	15 µm
Metric of Interest	Mean[Tsf[CY5]]

Table 8. Image preprocessing parameters.

Subpopulation Criteria			
Cell Subpopulation	**Channel**	**Metric of Interest**	**Positive Cell Cutoff Criteria**
Active mitochondria	RFP	Area_2[Tsf[RFP]]	>100 μm^2
Apoptosis	GFP	Mean_2[Tsf[GFP]]	>10000 RFU
Necrosis	CY5	Mean[Tsf[CY5]]	>2000 RFU

Results and discussion

Label-free total cell counting

High-contrast brightfield, label-free live cell imaging was performed to quantify total cell numbers throughout the 48-hour camptothecin incubation period. The focal plane of cells was automatically determined via laser autofocusing (Figure 26A), while an additional image was captured approximately 300 µm below the original focal plane (Figure 26B) and automatically preprocessed (Table 6) to increase cellular contrast (Figure 26C). Quantitative analysis was then performed using the total cell primary analysis parameters in Table 7, placing object masks around cells (Figure 26D), to determine total cell numbers per image.

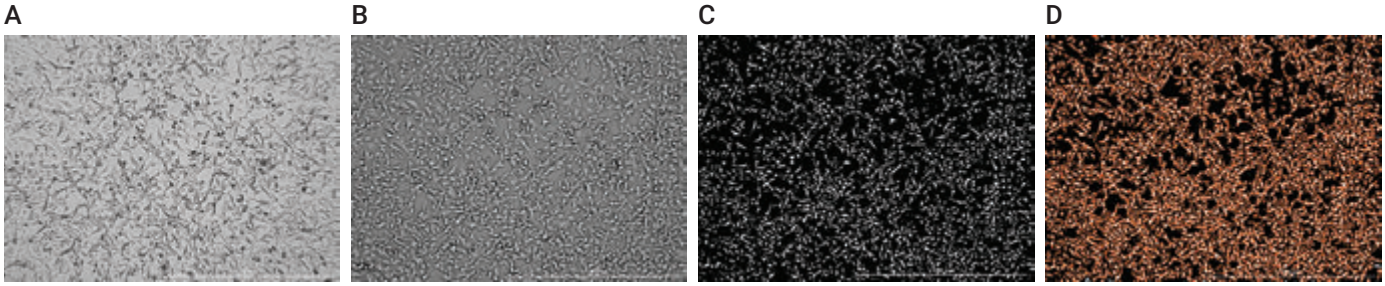

Figure 26. High-contrast brightfield image capture, preprocessing, and analysis. (A) 4x in-focus image of total HT-1080 cells. (B) 4x off-focus image of total HT-1080 cells. (C) Preprocessing of off-focus image. (D) Cellular analysis of preprocessed image. Object masks (in red) placed around total cells within image.

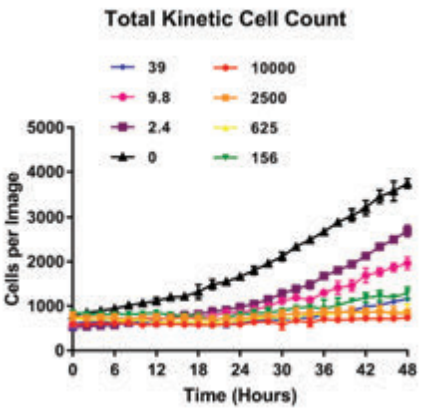

Figure 27. Kinetic HT-1080 total cell dose response curves. Average cell number per image was calculated from three replicate wells of each compound treatment at each timepoint. Camptothecin concentrations were as follows: 10,000 nM, 2,500 nM, 625 nM, 156 nM, 39 nM, 9.8 nM, 2.4 nM, 0 nM.

Results from the kinetic total cell analysis (Figure 27) confirmed the effect that increasing camptothecin concentrations have on HT-1080 cell proliferation. The accurate cell counts also demonstrate how primary cell analysis using high-contrast brightfield can be used as a normalization of positively affected cell counts.

Mitochondrial membrane potential

The TMRE cell permeant dye was added at time 0 to monitor mitochondrial membrane potential. As the dye is positively charged, it readily accumulated in negatively charged mitochondria, whereas depolarized mitochondria have decreased membrane potential and did not sequester the dye. The Cytation 5 RFP imaging channel was used to capture signal from the TMRE probe. Cells at time 0 (Figure 28A) contained active mitochondria leading to large areas of cytoplasmic probe signal. Loss of mitochondrial membrane integrity lead to diminished probe expression and smaller areas of cytoplasmic signal (Figure 28B). Active mitochondria cell secondary cellular analysis (Table 7) placed object masks around the TMRE probe RFP signal (Figures 28C and 28D). By setting minimum object area criteria (Table 8), the number of active mitochondrial cells per image over time was then determined (Figure 28E). This number was then normalized by dividing by previously determined total cell numbers to calculate kinetic active mitochondria cell percentages (Figure 28F).

The plotted curves in Figures 28E and 28F validated the known phenomenon that camptothecin induces cell death by negatively impacting mitochondrial membrane integrity.[24] Furthermore, these results confirmed the ability of the BioSpa and Gen5 to deliver accurate results using the TMRE live cell mitochondrial membrane potential probe.

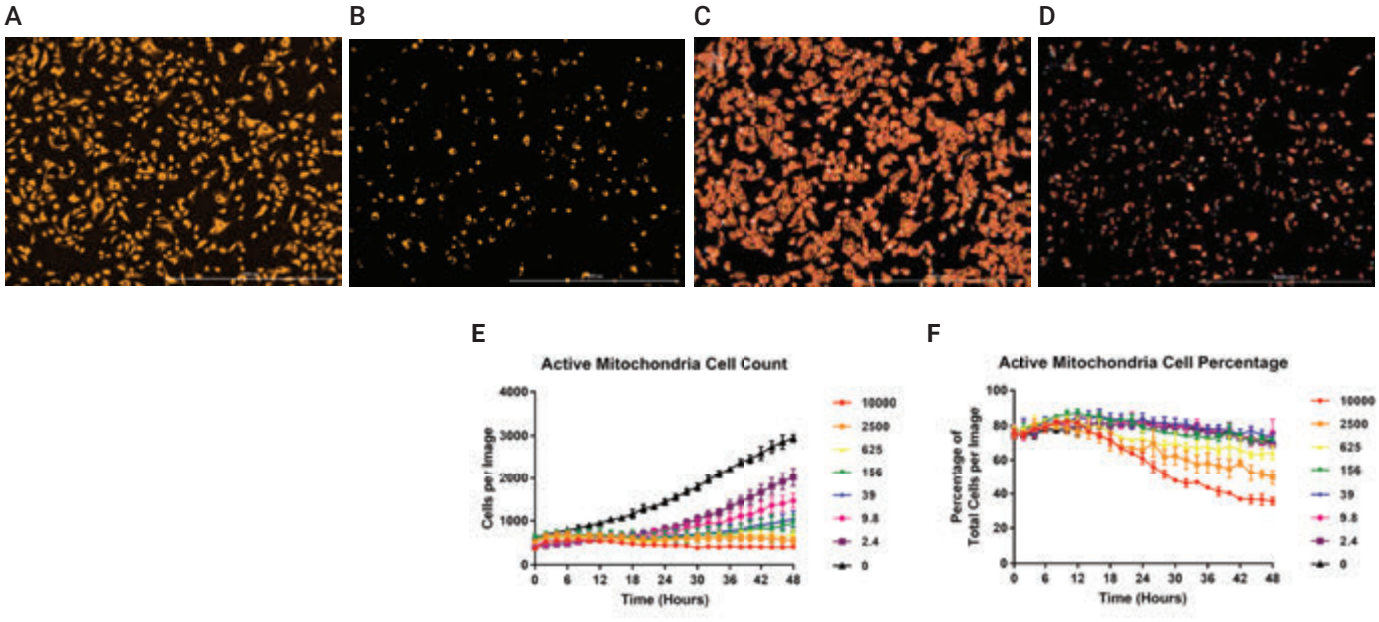

Figure 28. Active mitochondria imaging and analysis. Images captured with a 4x objective and RFP imaging channel following incubation periods of (A) 0 hours; and (B) 48 hours with 2,500 nM camptothecin. Cellular analysis was performed to place secondary masks around active mitochondria signal from cells treated with 2,500 nM camptothecin for (C) 0, and (D) 48 hours. White: Preprocessed high-contrast brightfield cellular areas. Orange: TMRE cytoplasmic signal. Red: Object masks. Kinetic curves were then plotted for (E) total active mitochondrial cells, and (F) mitochondrial cell percentages per image.

Apoptotic external phosphatidylserine exposure

Phosphatidyserine (PS) is a phospholipid that resides on the cytoplasmic surface of healthy cell membranes, and translocates to the outer membrane in the early stages of apoptosis. The reversible binding probe, Polarity sensitive indicator of viability and apoptosis (pSIVA), binds to externally exposed PS to create an intense green signal, and releases when PS internalizes. The GFP imaging channel was used to detect the pSIVA fluorescent signal as it increased upon camptothecin incubation with cells Figures 28A and 28B). Apoptotic cell secondary cellular analysis (Table 7) placed object masks around cytoplasmic pSIVA probe GFP signal (Figures 28C and 28D).

As the signal from the pSIVA probe upon apoptotic induction is independent of area, minimum object mean criteria (Table 8) identified apoptotic cells over time (Figure 29E) which was again normalized to total cell counts (Figure 29F). These graphs confirmed the ability of the imaging and analysis to detect and quantify camptothecin induced pSIVA apoptotic signal in a multiplexed setting.

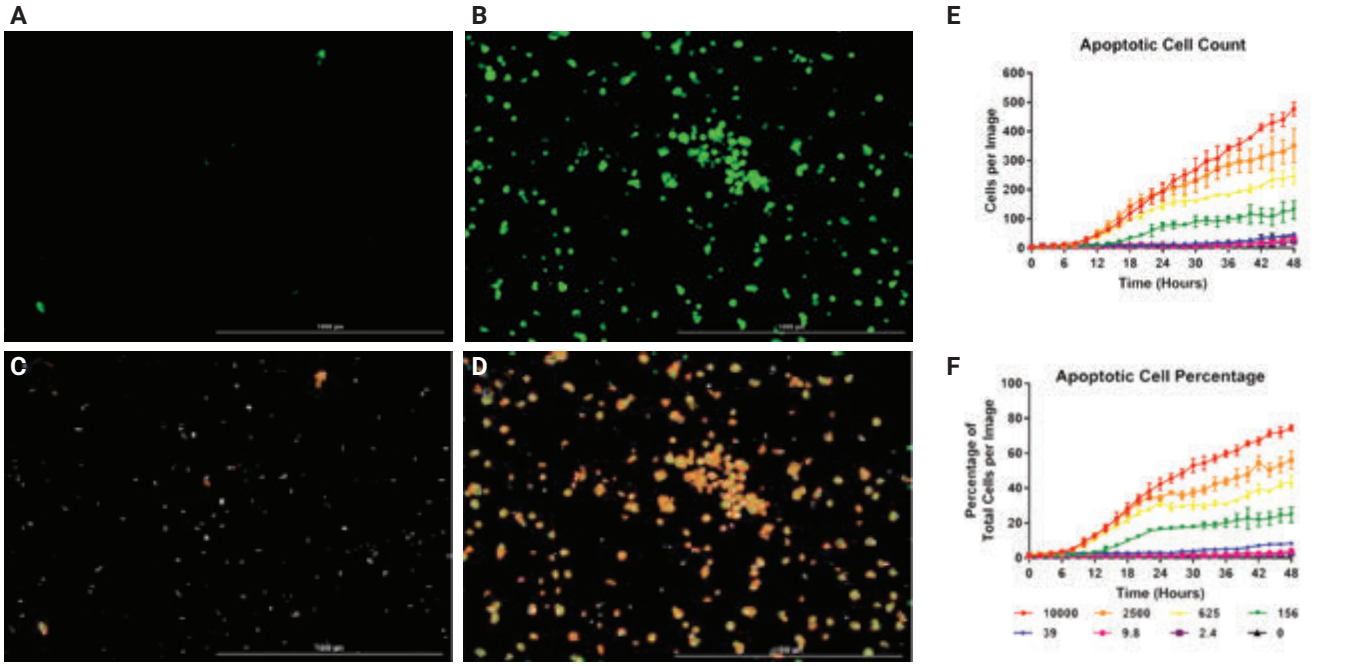

Figure 29. Apoptosis imaging and analysis. Images captured with a 4x objective and GFP imaging channel following incubation periods of (A) 0 hours; and (B) 48 hours with 2,500 nM camptothecin. Cellular analysis performed to place secondary masks around pSIVA signal from cells treated with 2,500 nM camptothecin for (C) 0, and (D) 48 hours. White: Preprocessed high-contrast brightfield cellular areas; green: pSIVA cytoplasmic signal; Red: object masks. Kinetic curves then plotted for (E) total apoptotic cells, and (F) apoptotic cell percentages per image.

Necrotic cell membrane integrity loss

The far-red cell impermeant dye, Deep Red Anthraquinone 7 (DRAQ7), binds to cell nuclei upon loss of cell membrane integrity, an indication of necrosis, to create a red fluorescent signal that was captured using the CY5 imaging channel. Similar to pSIVA, DRAQ7 fluorescent signal increased upon camptothecin incubation with cells (Figures 29A and 29B). Necrotic cell secondary cellular analysis (Table 7)

placed object masks around the nuclear probe CY5 signal. Minimum object mean criteria (Table 8) again identified necrotic cells over time and was normalized to total cell counts (Figure 30C). This graph further validated the ability of the imaging and analysis to detect and quantify camptothecin induced changes in TMRE, pSIVA, and DRAQ7 signals from a single well in a multiplexed setting.

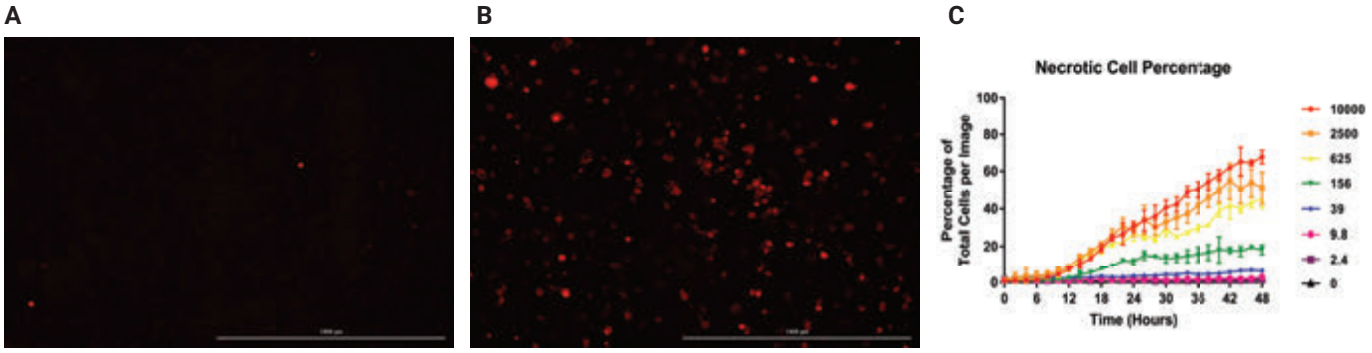

Figure 30. Necrosis imaging and analysis. Images captured with a 4x objective and CY5 imaging channel following incubation periods of (A) 0 hours; and (B) 48 hours with 2,500 nM camptothecin. (C) Necrotic cell percentages per image following primary and secondary cellular analysis.

Variable incubation analysis comparison

An advantage of the BioSpa is the ability to monitor the effect of camptothecin treatment, not only at one particular timepoint, but at regular intervals kinetically over extended incubation periods. Per Figure 31, the calculated EC_{50} values generated from dose response curves plotted from necrotic cell percentages determined following 0-, 12-, 24-, and 48-hour camptothecin treatments illustrated that short-term incubations can lead to false assumptions about the true potency of test molecules. By incorporating kinetic analysis, accurate conclusions can be determined.

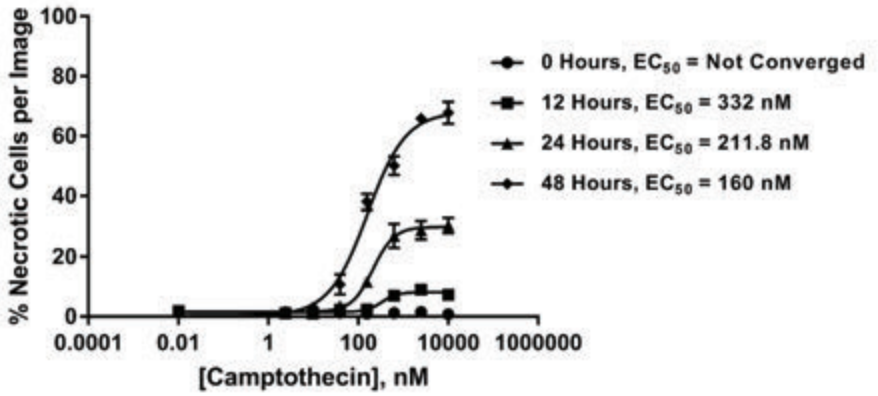

Figure 31. Camptothecin percent necrotic cell per image dose response curves. Induced necrotic cell percentage per image curves following camptothecin incubations of 0, 12, 24, and 48 hours.

The multiple fluorescent imaging detection channels on the Cytation 5 allow the live cell TMRE, pSIVA, and DRAQ7 probes to be multiplexed within the same well, providing a simple and robust method to measure multiple cell death pathways.

Proper environmental conditions provided by the BioSpa then allows for images to be captured automatically over extended incubation periods, improving the ability to gain a more complete picture of the effect of each test molecule. Finally, by incorporating cellular analysis techniques with Gen5 software, accurate conclusions can be deduced by viewing normalized kinetic induction curves, as well as the response from multiple test concentrations over time.

Recent publications using Agilent BioTek microscopes for labeled measurements of cell proliferation, viability, apoptosis, and necrosis

1. K. Baergen, L. M. Jeusset, Z. Lichtensztejn, and K. J. McManus, "Diminished Condensin Gene Expression Drives Chromosome Instability That May Contribute to Colorectal Cancer Pathogenesis," *Cancers, vol. 11, no. 8, p. 1066,* Jul. **2019**, doi: 10.3390/cancers11081066.
2. C. Lepage, L. L. Thompson, B. Larson, and K. J. McManus, "An Automated, Single Cell Quantitative Imaging Microscopy Approach to Assess Micronucleus Formation, Genotoxicity and Chromosome Instability," *Cells, vol. 9, no. 2, p. 344,* Feb. **2020**, doi: 10.3390/cells9020344.
3. E. N. McAndrew, C. C. Lepage, and K. J. McManus, "The synthetic lethal killing of RAD54B-deficient colorectal cancer cells by PARP1 inhibition is enhanced with SOD1 inhibition," *Oncotarget, vol. 7, no. 52,* Dec. **2016**, doi: 10.18632/oncotarget.13654.
4. H. I. Muendlein et al., "cFLIP L protects macrophages from LPS-induced pyroptosis via inhibition of complex II formation," *Science, vol. 367, no. 6484, pp. 1379–1384*, Mar. **2020**, doi: 10.1126/science.aay3878.
5. H. I. Muendlein et al., "Constitutive Interferon Attenuates RIPK1/3-Mediated Cytokine Translation," *Cell Rep., vol. 30, no. 3, pp. 699-713.e4,* Jan. **2020**, doi: 10.1016/j.celrep.2019.12.073.
6. V. Sajesh and K. J. McManus, "Targeting SOD1 induces synthetic lethal killing in BLM- and CHEK2-deficient colorectal cancer cells," *Oncotarget, vol. 6, no. 29,* Sep. **2015**, doi: 10.18632/oncotarget.4875.
7. J. Sarhan et al., "Caspase-8 induces cleavage of gasdermin D to elicit pyroptosis during Yersinia infection," *Proc. Natl. Acad. Sci., vol. 115, no. 46, pp. E10888–E10897,* Nov. **2018**, doi: 10.1073/pnas.1809548115.
8. Singh et al., "The BH3 only Bcl-2 family member BNIP3 regulates cellular proliferation," *PLOS ONE, vol. 13, no. 10, p. e0204792,* Oct. **2018**, doi: 10.1371/journal.pone.0204792.

Monitoring *Saccharomyces cerevisiea* growth with brightfield microscopy in real time

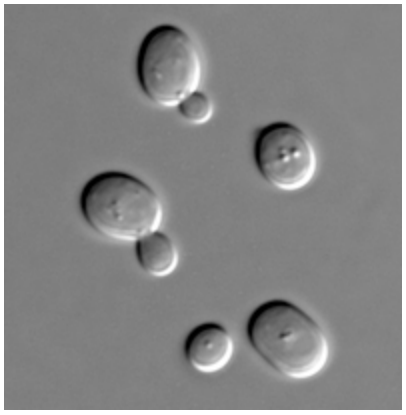

Figure 32. *Saccharomyces cerevisiea.*

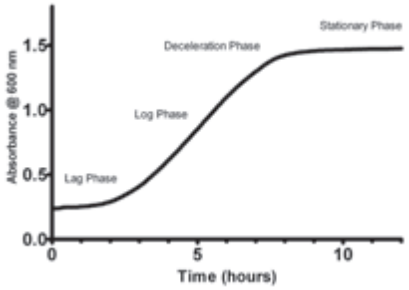

Figure 33. Typical yeast growth curve. *Saccharomyces cerevisiea* suspensions grown in YPD media at 30 °C for 12 hours with data measurements every two minutes using an Agilent BioTek Synergy H1 multimode reader.

Assay principle

Yeast are single celled eukaryotic fungi organisms that reproduce asexually by budding or division (Figure 32). While yeast can vary in size, they typically measure 3-8 µm in diameter. *Saccharomyces cerevisiea* is the most commonly used strain in scientific research, baking and fermentation and has become synonymous with the term yeast.

When cultured in a fixed environment, yeast cells follow a very predictable pattern of growth that can easily be divided into four phases: (1) lag; (2) log; (3) deceleration; and (4) stationary. During the lag phase, no growth occurs, as newly introduced yeast mature and acclimate to the environment. This is followed by the log phase, where cells are rapidly growing and dividing. Nutrients are in excess relative to cell number, and waste is being sufficiently diluted as to be insignificant. The growth rate in this phase follows first-order kinetics. As cell numbers increase, cell growth begins to slow as a number of parameters (e. g. substrate and waste), each with saturation effects, become significant. Eventually the yeast cells reach the stationary phase, where no growth occurs due to high waste concentration or complete substrate consumption (Figure 33).

Unfortunately, these different stages make interpretation of growth data difficult. Growth rates in a static environment are a function of not only the ability of the yeast cell to grow, but also environmental conditions such as depletion of nutrients or the accumulation of waste byproducts. Using a perfusion system allows for the maintenance of proper growth nutrients, as well as elimination of waste products as they are produced, with growth limited only by physical space.

Yeast growth experiments are often performed in microplates using light scatter vertical photometry, which allows for a large number of different experimental conditions to be tested rapidly. This format, which makes indirect measurements of cell number, can suffer when cell yeast cell suspensions flocculate and can no longer remain suspended, forming opaque clumps on the bottom of the well. This phenomenon results in aberrantly high absorbance levels, making analysis difficult if not impossible. Because this technique uses light scatter rather than true absorbance, measurements made with different optics (i.e. different reader types) will result in different values. Likewise, comparison of different yeast strains, with different sizes, can often be problematic as cell size has a substantial influence on light scatter.

Classic ONYX plate

The ONIX Y04C-02 microfluidic plate is a 4-chamber cell culture plate designed to be used with the ONIX2 Microfluidic System for perfusion studies with haploid yeast cells. The Y04C plate has 4 independent units (A-D), each with 6 inlet wells (1-6), a cell inlet (8), and a large outlet well (7). Each row of wells (A-D) addresses the corresponding culture chamber (Figure 34).

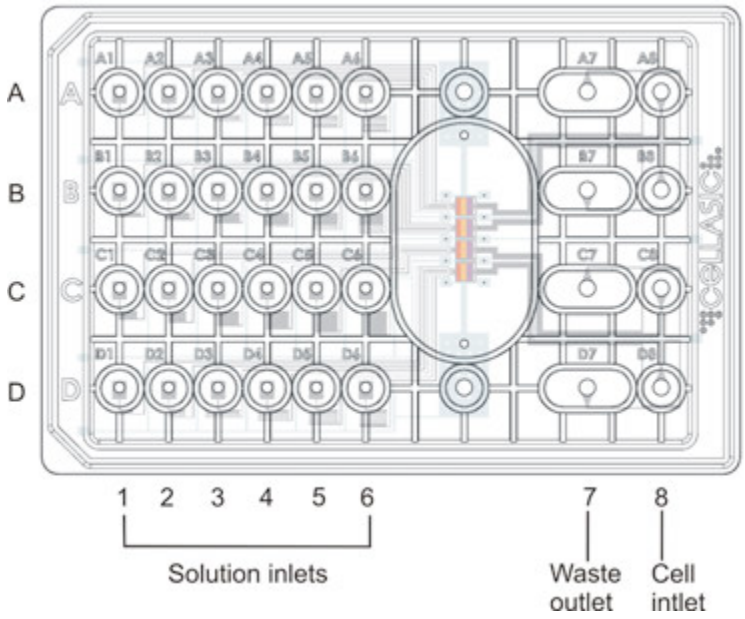

Figure 34. ONIX CellASIC plate configuration.

All four culture chambers are located in a single viewing window to minimize imaging objective X-Y travel. Each has 6 separate microfluidic inlets to provide reagents and growth media (Figure 35).

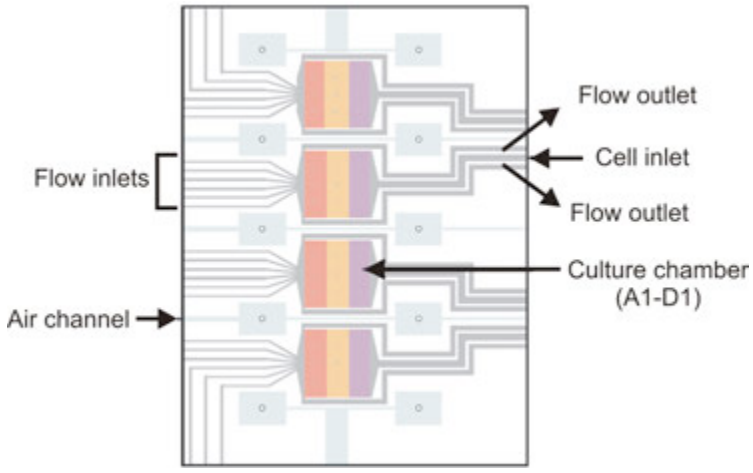

Figure 35. CellASIC chamber viewing window. The CellASIC has four completely separate viewing cells, each with 6 different inlet sources for perfusion fluids. Viewing chamber C1 is identified.

Each chamber is 3.0 mm x 3.0 mm in area with different heights (3.5, 4.0, 4.5 µm) between the glass and the upper ceiling. The trap heights decrease in distance as one moves across the chamber from the inlet source for cells (Figure 36).

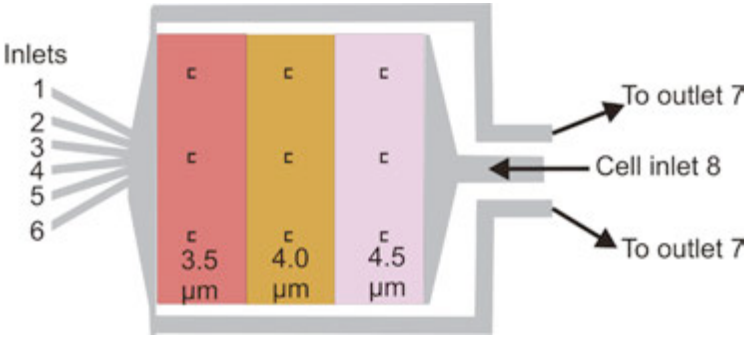

Figure 36. Culture chamber. The culture chamber has nine position markers "c" in conjunction with three different trap heights.

Each viewing chamber uses an elastic ceiling that holds the cells against the imaging glass surface to maintain a single focal plane. As cells are driven with pressure across the viewing chamber they will eventually be trapped and stabilized between the elastic ceiling and the glass imaging surface (Figure 37).

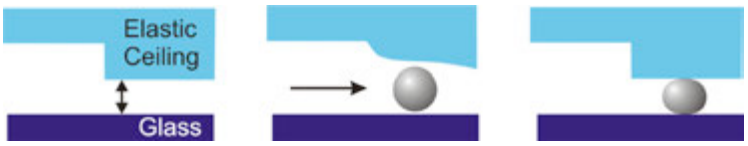

Figure 37. Cell trapping mechanism.

Materials and methods

BactoYeast extract, dextrose, BactoPeptone, sodium chloride, monobasic and dibasic phosphate powders, and ethanol were obtained from Sigma-Aldrich (St. Louis, MO). Yeast strain By4742 was obtained from ATCC (part number 4012458). Yeast Extract-Peptone-Dextrose (YPD) media was prepared, by dissolving 10 g BactoYeast extract, 20 g BactoPeptone and 20 g Dextrose in 1 liter of water and sterilized by autoclaving. Dilution of YPD, if necessary, were made with Milli Q water or the indicated reagent.

All experiments followed the same general format. Yeast overnight stock cultures using YPD media (50 mL) were grown in 250 mL Erlenmeyer flasks at 30 °C with orbital shaking at 125 RPM. Prior to growth experiments, 100 µL of each overnight stock culture was diluted to 9.9 mL with fresh 1x YPD media. The diluted cells (50 µL) were then loaded into CellASIC Y04C-02 plates using the cell inlet wells (position 8). Reagents were loaded into solution inlets (positions 1-6) as required for the experiment. Perfusion timing and rate were controlled using the ONIX2 Microfluidic System (Millipore-Sigma). Perfusion pressure was set to 10 kPa, with perfusion beginning immediately after loading unless indicated.

Imaging

Montage brightfield images (2x2) were made kinetically every 5 minutes for 12 hours using an Agilent BioTek Lionheart FX automated microscope fitted with a 20x objective. Camera exposure settings were optimized manually at the beginning of each experiment and image focusing was maintained using laser autofocusing. Temperature control was enabled and unless stated otherwise was at 30 °C.

Analysis

The montage brightfield images were stitched using a linear blend fusion method. Cell growth was assessed by object mask counting of the stitched brightfield images to identify yeast cells. Background selection was set to "Light" with a rolling ball diameter of 3 µm for background flattening. The mask threshold set to 4,500, with object smaller than 1 µm or larger than 10 µm being excluded.

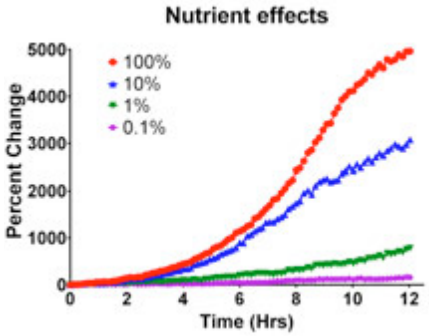

Figure 38. Effect of nutrient concentration on yeast cell growth.

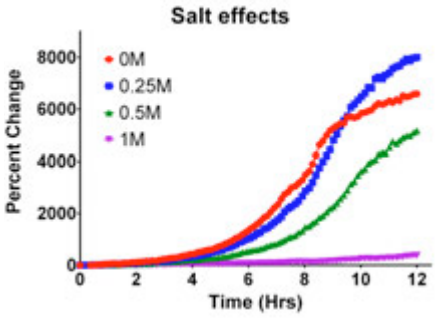

Figure 39. Effect of ionic strength on yeast cell growth. Yeast cells were perfused with YPD media containing various concentrations of sodium chloride and the cells imaged with brightfield. Image analysis cell counts were plotted as a function of time. Each data point represents a time point from a single viewing chamber.

Results and discussion

Media concentration

The effect of nutrient concentration on cell growth was examined by dilution of the YPD media. Undiluted YPD (100 %) was diluted in a series of 1:10 dilutions with water and perfused into the viewing chamber. As demonstrated in Figure 38, the dilution of the growth nutrients has a marked effect on cellular growth rate. As nutrients in the media are diluted with water, cell proliferation decreases dramatically. Perfusion with YPD diluted 1,000-fold results in virtually no growth over 12 hours while complete media returns a 5,000 percent increase in the number of cells over the same period.

Salt sensitivity

Ionic strength of the growth media is a concern when yeast cells are propagated in mixtures not consisting of formulated nutrients diluted with deionized or distilled water. For example, remediation of contaminated water or the fermentation of cellulosic digests can vary and possibly contain large amounts of ions.

Yeast cells show a great deal of tolerance in regards to growth in the presence of high sodium chloride concentrations (Figure 39). The effect of ionic strength on yeast cell growth was assessed by perfusing loaded cells with YPD-containing exogenous NaCl. Four dilutions of NaCl were added such that the final sodium chloride concentration ranged from 0 to 1 M. The concentration of YPD was equivalent (90 %) in all chambers. While high-salt concentrations (1M) effectively stop cell proliferation, yeast perfused with 0.5 M sodium chloride was able to grow to a concentration nearly 80 % that of untreated yeast cultures. Lower salt conditions allowed cell growth that was equivalent to or slightly better than untreated cells.

pH sensitivity

In order to test the effect of pH on yeast cell growth, cultures of *Saccharomyces cerevisiea* were perfused with YPD supplemented with 20 mM phosphate at pH ranging from 4.5 to 9.5. In all cultures YPD comprised 80 % of the mixture and the phosphate buffer the remaining 20 % by volume.

Yeast has a propensity to grow much better in acidic conditions as compared to alkali. This is demonstrated in Figure 40, where cells perfused with pH 4.5 YPD mixtures grow to concentrations nearly twice that of pH 7.5 media. Alkaline mixtures (pH 9.5) exhibited substantially slower growth than acidic cultures, but still managed to replicate.

Ethanol tolerance

Yeast produces ethanol and carbon dioxide as byproducts of the fermentation of sugars. As the concentration of waste byproducts becomes significant its presence can become a detriment to cell growth. When the influence of ethanol is examined, it becomes apparent that high levels of ethanol are inhibitory to yeast growth with strain By4742. These cells are quite tolerant to ethanol levels of 1 % or less. Above these levels a marked decrease in the growth of the yeast strain is observed (Figure 41).

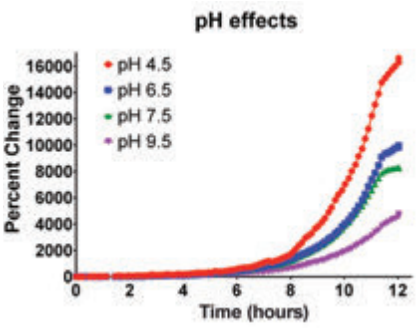

Figure 40. Effect of pH on yeast cell growth. Yeast cells were loaded into a CellASIC plate and perfused with YPD (80 %) containing phosphate buffer at various pH levels. Data represents the percent change in cell number from the initial reading. Each data point represents an unique time point from a single viewing chamber.

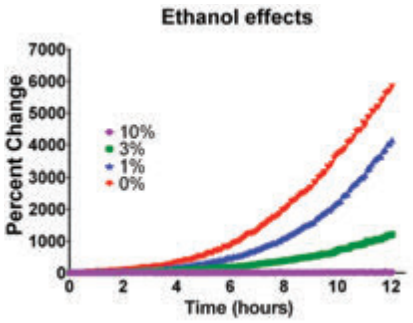

Figure 41. Effect of ethanol on yeast cell growth. Yeast cells were loaded into a CellASIC plate and perfused with YPD (90 %) containing various concentrations of ethanol. Data represents the percent change in cell number from the initial reading. Each data point represents a time point from a single viewing chamber.

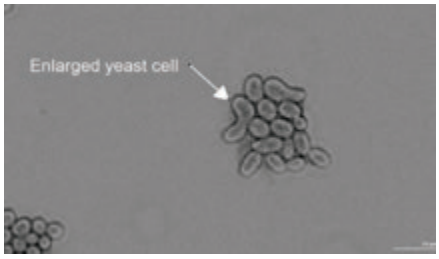

Figure 42. Brightfield image of cell cycle arrested *Saccharomyces cerevisiea* cells. Yeast cells treated with 30 µM nocodazole for three hours were imaged in brightfield using a 60x air objective.

Nocodazole exposure

Nocodazole is a potent antineoplastic agent which exerts its effects by interfering with the polymerization of microtubules.[25] In budding yeast it stalls cells in the G2/M phase of the cell cycle resulting in large buds that do not detach from the mother cell (Figure 42).

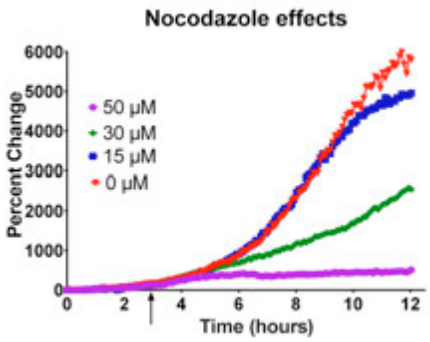

Figure 43. Kinetic growth curves of yeast cells perfused with nocodazole. Yeast were loaded into the CellASIC plate and immediately perfused with YPD media. After three hours, the perfusion mixture was changed to include various concentrations of nocodazole in YPD. The initiation of nocodazole perfusion is indicated by the arrow. Data points reflect the percent change for the initial cell count for a single viewing chamber.

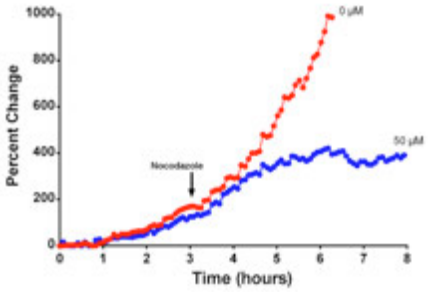

Figure 44. Comparison of cell counts of *Saccharomyces cerevisiea* perfused with either 0 µM or 50 µM nocodazole. Yeast cells were loaded onto CellASIC plates and allowed to grow with YPD media perfusion. After three hours the perfusion mixture was changed to YPD containing either 0 µM or 50 µM nocodazole. Data reflects the kinetic cell counts from separate cells.

Budding daughter yeast cells stalled in G2/M often do not detach from the mother cell and typically exhibit an enlarged phenotype. This phenomenon can be observed as a decrease in cell proliferation. As demonstrated in Figure 12, cell cycle blockage by nocodazole is concentration-dependent. Cells exposed to 50 µM nocodazole virtually stop proliferating shortly after exposure. With lower concentrations a decrease in cell proliferation is observed (Figure 43).

The effectiveness of perfusion is demonstrated in Figure 44. Yeast cells seeded into the CellASIC plate and perfused with YPD media increase in number through cell budding. Shortly after the initiation of perfusion with 50 µM nocodazole, cultures stop dividing and cell number no longer increases. Cultures seeded at the same time, but continue budding and cell numbers rapidly increase.

These data demonstrate the ability of the Lionheart FX in conjunction with the ONIX2 Microfluidic Platform to quantitate yeast growth by cell counting. The CellASIC Y04C plate uses different size traps to immobilize mother cells for repeated imaging. Brightfield imaging, followed by digital image analysis, allows for cell quantitation in real time.

Perfusion of cultures provides a means to not only add fresh nutrients, but to also remove waste products. A case in point is the production of ethanol by formation. This waste product can build up to levels that will effectively eliminate growth independent of the availability of nutrients. The removal of this byproduct by a continuous flow system can conceivably prevent the stationary phase resulting from byproduct buildup. In the context of strain development, this would bypass the need to develop ethanol resistance.

In a general sense, the use of perfusion allows for unabated growth resulting in the almost complete elimination of the stationary phase observed with static experiments where nutrients are not added and wastes are not continually removed. When the viewing region chamber is completely filled, cell counts begin to level off as cell growth pushes cells out of the imaging area. Imaging using larger montages can be used to lengthen the experimental window.

These data demonstrate that both environmental, as well as drug induced changes in yeast cell growth can be monitored using the Lionheart FX in conjunction with the ONIX2 Microfluidic Platform. Note that the data is actual cell number rather than an indirect measurement based on light scatter. These experiments used lengthy kinetic runs to analyze the capability of the yeast strains. An important point to note is that, despite markedly different growth rates, some of the different culture conditions resulted in the same final cell density. This is a finding that an end point determination at the end of a long incubation would have missed. The data analysis was simplified by the ability of Gen5 to automatically count yeast cells in real time.

Recent publications using Agilent BioTek microscopes for measuring proliferation of non-mammalian cells

1. C. Garcia, A. Burgain, J. Chaillot, É. Pic, I. Khemiri, and A. Sellam, "A phenotypic small-molecule screen identifies halogenated salicylanilides as inhibitors of fungal morphogenesis, biofilm formation and host cell invasion," *Sci. Rep., vol. 8, no. 1, p. 11559,* Dec. **2018**, doi: 10.1038/s41598-018-29973-8.
2. D. A. Hanna, R. Hu, H. Kim, O. Martinez-Guzman, M. P. Torres, and A. R. Reddi, "Heme bioavailability and signaling in response to stress in yeast cells," *J. Biol. Chem., vol. 293, no. 32, pp. 12378–12393,* Aug. **2018**, doi: 10.1074/jbc.RA118.002125.

References

1. L. A. Harris et al., "An unbiased metric of antiproliferative drug effect *in vitro*," *Nat. Methods, vol. 13, no. 6, pp. 497–500,* Jun. **2016**, doi: 10.1038/nmeth.3852.
2. M. Niepel, M. Hafner, M. Chung, and P. K. Sorger, "Measuring Cancer Drug Sensitivity and Resistance in Cultured Cells: Cancer Drug Sensitivity and Resistance in Cells," *Curr. Protoc. Chem. Biol., vol. 9, no. 2, pp. 55–74,* Jan. **2017**, doi: 10.1002/cpch.21.
3. A. Adan, Y. Kiraz, and Y. Baran, "Cell Proliferation and Cytotoxicity Assays," *Curr. Pharm. Biotechnol., vol. 17, no. 14, pp. 1213–1221,* Nov. **2016,** doi: 10.2174/1389201017666160808160513.
4. K. Präbst, H. Engelhardt, S. Ringgeler, and H. Hübner, "Basic Colorimetric Proliferation Assays: MTT, WST, and Resazurin, in Cell Viability Assays: Methods and Protocols", *D. F. Gilbert and O. Friedrich, Eds. New York, NY: Springer New York, pp. 1–17,* **2017**.
5. W. Strober, "Trypan Blue Exclusion Test of Cell Viability," *Curr. Protoc. Immunol., vol. 21, no. 1, p. A.3B.1-A.3B.2,* **1997**, doi: 10.1002/0471142735.ima03bs21.
6. D. I. Pattison and M. J. Davies, "Actions of ultraviolet light on cellular structures," *in Cancer: Cell Structures, Carcinogens and Genomic Instability, Basel: Birkhäuser, pp. 131–157,* **2006**.
7. L. L. Drey, M. C. Graber, and J. Bieschke, "Counting unstained, confluent cells by modified bright-field microscopy," *BioTechniques, vol. 55, no. 1, pp. 28–33,* Jul. **2013**, doi: 10.2144/000114056.
8. P. Held and P. Banks, "High Contrast Brightfield: Enabling microplate-based automated label-free cell counting," *BioTek Resources,* **2016**.
9. J. Clayton and P. Banks, "A Guide to Label-free Cell Counting using High Contrast Brightfield," *BioTek Resources,* **2016**.
10. O. Tacar, P. Sriamornsak, and C. R. Dass, "Doxorubicin: an update on anticancer molecular action, toxicity and novel drug delivery systems: Doxorubicin cell and molecular biological activity," *J. Pharm. Pharmacol., vol. 65, no. 2, pp. 157–170*, Feb. **2013**, doi: 10.1111/j.2042-7158.2012.01567.x.
11. F. A. Fornari, J. K. Randolph, J. C. Yalowich, M. K. Ritke, and D. A. Gewirtz, "Interference by doxorubicin with DNA unwinding in MCF-7 breast tumor cells," *Mol. Pharmacol., vol. 45, no. 4, pp. 649–656,* Apr. **1994**.

12. B. W. Konicek et al., “Therapeutic Inhibition of MAP Kinase Interacting Kinase Blocks Eukaryotic Initiation Factor 4E Phosphorylation and Suppresses Outgrowth of Experimental Lung Metastases,” *Cancer Res., vol. 71, no. 5, pp. 1849–1857,* Mar. **2011**, doi: 10.1158/0008-5472.CAN-10-3298.
13. J. K. Altman et al., “Inhibition of Mnk kinase activity by cercosporamide and suppressive effects on acute myeloid leukemia precursors,” *Blood, vol. 121, no. 18, pp. 3675–3681,* May **2013**, doi: 10.1182/blood-2013-01-477216.
14. J. Clayton, “Kinetic Proliferation Assay Using Label-Free Cell Counting,” *BioTek Instrum. Appl. Note,* **2017**, [Online]. Available: https://www.biotek.com/resources/application-notes/kinetic-proliferation-assay-using-label-free-cellcounting/.
15. R. Rhoades and D. R. Bell, Medical physiology: principles for clinical medicine. **2013.**
16. Y. Berthois, J. A. Katzenellenbogen, and B. S. Katzenellenbogen, “Phenol red in tissue culture media is a weak estrogen: implications concerning the study of estrogen-responsive cells in culture.,” *Proc. Natl. Acad. Sci., vol. 83, no. 8, pp. 2496–2500,* Apr. **1986**, doi: 10.1073/pnas.83.8.2496.
17. P. Held, “Using Phenol Red to assess pH in Tissue Culture Media,” BioTek Instrum. Appl. Note, [Online]. Available:https://www.biotek.com/resources/application-notes/using-phenol-red-to-assess-ph-in-tissue-culture-media/.
18. D. Hanahan and R. A. Weinberg, “Hallmarks of Cancer: The Next Generation,” *Cell, vol. 144, no. 5, pp. 646–674,* Mar. **2011**, doi: 10.1016/j.cell.2011.02.013.
19. L. Galluzzi et al., “Molecular mechanisms of cell death: recommendations of the Nomenclature Committee on Cell Death 2018,” *Cell Death Differ., vol. 25, no. 3, pp. 486–541,* Mar. **2018**, doi: 10.1038/s41418-017-0012-4.
20. K. Segawa and S. Nagata, “An Apoptotic ‘Eat Me’ Signal: Phosphatidylserine Exposure,” *Trends Cell Biol., vol. 25, no. 11, pp. 639–650,* Nov. **2015**, doi: 10.1016/j.tcb.2015.08.003.
21. Y. E. Kim, J. Chen, J. R. Chan, and R. Langen, “Engineering a polarity-sensitive biosensor for time-lapse imaging of apoptotic processes and degeneration,” *Nat. Methods, vol. 7, no. 1, pp. 67–73,* Jan. **2010**, doi: 10.1038/nmeth.1405.
22. M. S. Ricci and W.-X. Zong, “Chemotherapeutic approaches for targeting cell death pathways,” *The Oncologist, vol. 11, no. 4, pp. 342–357,* Apr. **2006**, doi: 10.1634/theoncologist.11-4-342.
23. S. K. Halonen, “Modulation of Host Programmed Cell Death Pathways by the Intracellular Protozoan Parasite, Toxoplasma gondii — Implications for Maintenance of Chronic Infection and Potential Therapeutic Applications,” *in Cell Death - Autophagy, Apoptosis and Necrosis, T. M. Ntuli, Ed. InTech*, **2015**.
24. C.-W. Zeng et al., “Camptothecin Induces Apoptosis in Cancer Cells via MicroRNA-125b-Mediated Mitochondrial Pathways,” *Mol. Pharmacol., vol. 81, no. 4, pp. 578–586,* Apr. **2012**, doi: 10.1124/mol.111.076794.
25. R. J. Vasquez, B. Howell, A. M. Yvon, P. Wadsworth, and L. Cassimeris, “Nanomolar concentrations of nocodazole alter microtubule dynamic instability *in vivo* and *in vitro*.,” *Mol. Biol. Cell, vol. 8, no. 6, pp. 973–985,* Jun. **1997**, doi: 10.1091/mbc.8.6.973.

Learn more:
www.agilent.com/lifesciences/biotek

Get answers to your technical questions and access resources in the Agilent Community:
community.agilent.com

Buy online:
www.agilent.com/chem/store

U.S. and Canada
1-800-227-9770
agilent_inquiries@agilent.com

Europe
info_agilent@agilent.com

Asia Pacific
inquiry_lsca@agilent.com

RA44173.6644675926

Published in the USA, February 1, 2021
5994-2568EN
AG082120_02

Agilent
Trusted Answers